QCD tests in pp collisions at $\sqrt{s} = 7$ TeV using the ATLAS detector at the LHC.

Javier Llorente Merino

Institute of High Energy Physics

Beijing, January 2016

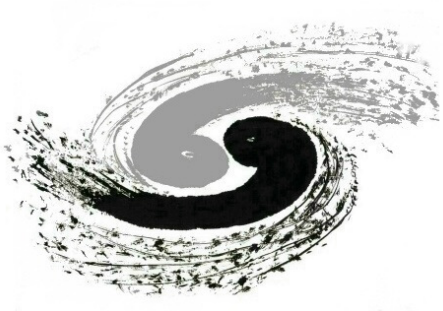

Outline of the talk

- Introduction.
  - Internal structure of hadronic jets: jet shapes.
  - Global event structure: event shapes.
- The ATLAS detector and jet reconstruction.
- Measurement of jet shapes in $t\bar{t}$ events.
  - The dead cone effect in heavy quark radiation
  - The $\ell^+\ell^-$ and $\ell^\pm q\bar{q}'$ $t\bar{t}$ event selections.
  - The light and b-jet samples.
  - Correction for detector effects.
- Determination of the b-quark mass.
  - The parton shower scale Λ_s.
  - The bottom mass m_b.
  - Theoretical uncertainties.
- Measurement of TEEC and determination of α_s.
  - Definition and properties.
  - Event selection and detector-level distributions.
  - Unfolding and systematic uncertainties.
  - Determination of the strong coupling.

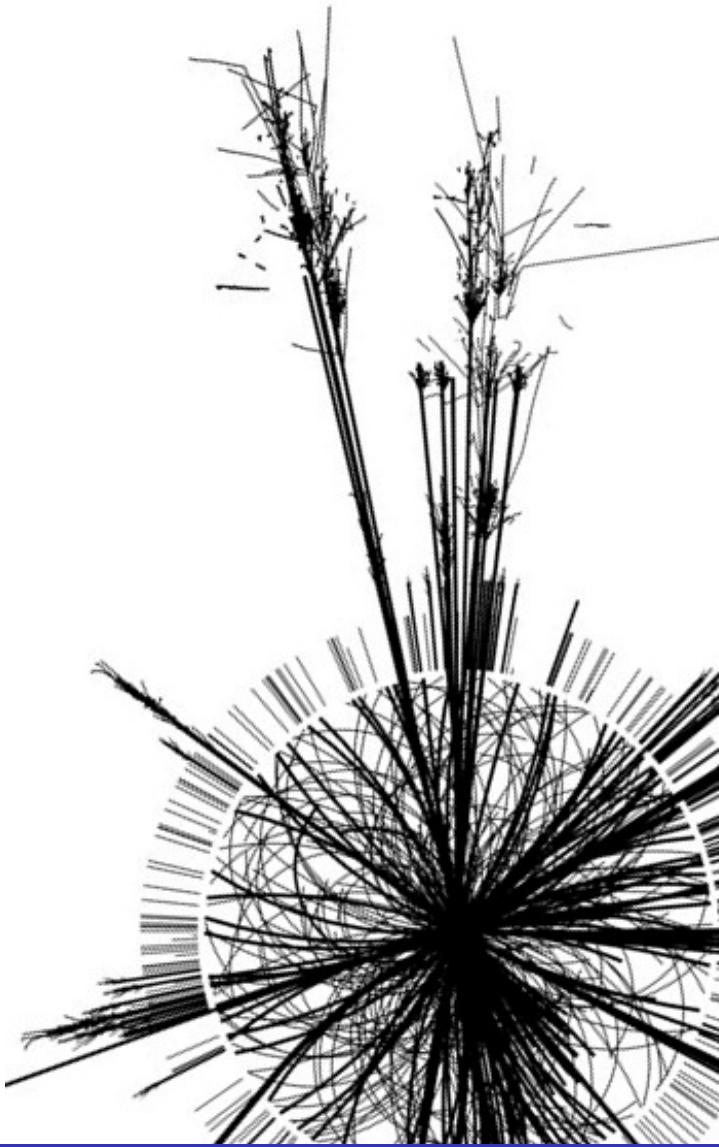

I. Introduction

$$\mathcal{L}_{\mathrm{QCD}} = -\frac{1}{4} F^a_{\mu\nu} F^{\mu\nu}_a + \sum_{j,k} \bar{\Psi}_j \left(i\gamma^\mu D_\mu - m \right)_{jk} \Psi_k$$

$$D_\mu = \partial_\mu - i g_s G^a_\mu(x) \lambda_a$$

$$F_{\mu\nu} = \frac{i}{g_s} [D_\mu, D_\nu]$$

$$\lambda_a \in \mathfrak{su}(3)$$

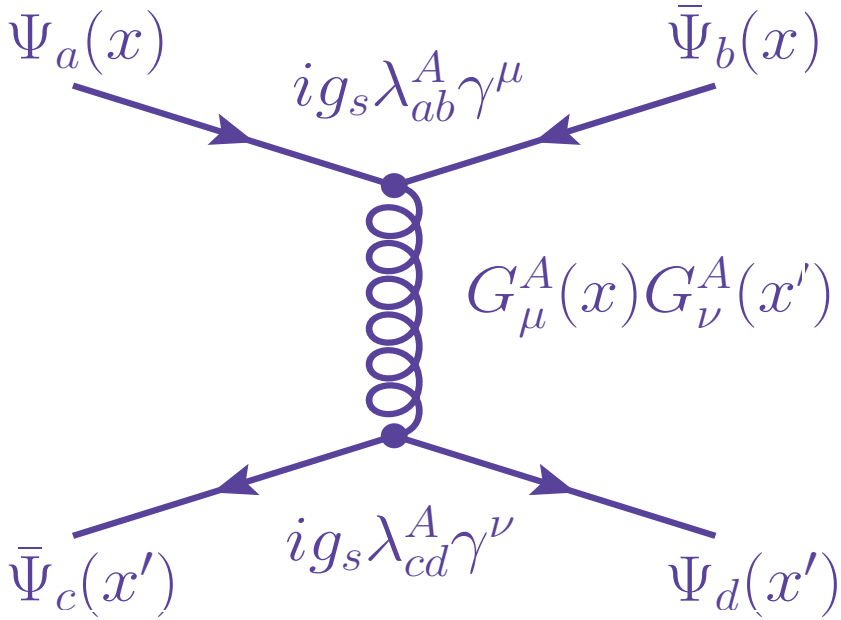

Internal structure of hadronic jets: jet shapes

- Jets: Collimated sprays of hadrons from the fragmentation of partons.
- Normalised momentum flow as a function of the distance to the jet axis.
- Sensitive observables for the modelling of the parton shower.

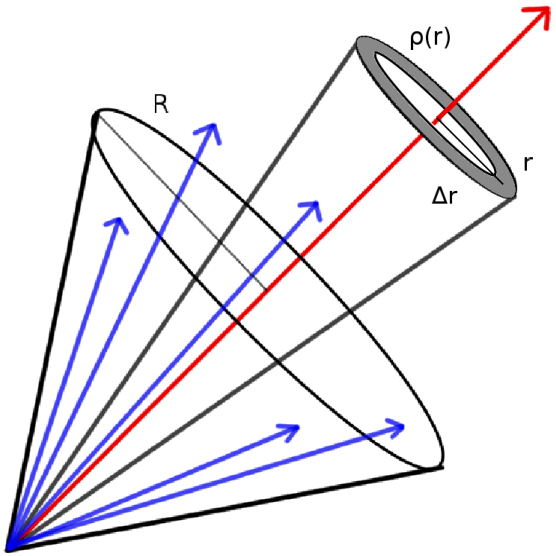

- Differential jet shape $r \leq R - \Delta r/2$

$$\rho(r) = \frac{1}{\Delta r} \frac{p_T(r - \Delta r/2, r + \Delta r/2)}{p_T(0, R)}$$

- Integrated jet shape $r \leq R$

$$\Psi(r) = \frac{p_T(0, r)}{p_T(0, R)}$$

Historical perspective: jet shapes in *ep* DIS

Precise way of testing QCD [ZEUS Collaboration, Nucl. Phys. B 700 3 (2004)]

$$\alpha_s(M_Z) = 0.1176 \pm 0.0009\ (\text{stat.})^{+0.0009}_{-0.0026}\ (\text{exp.})^{+0.0091}_{-0.0072}\ (\text{th.})$$

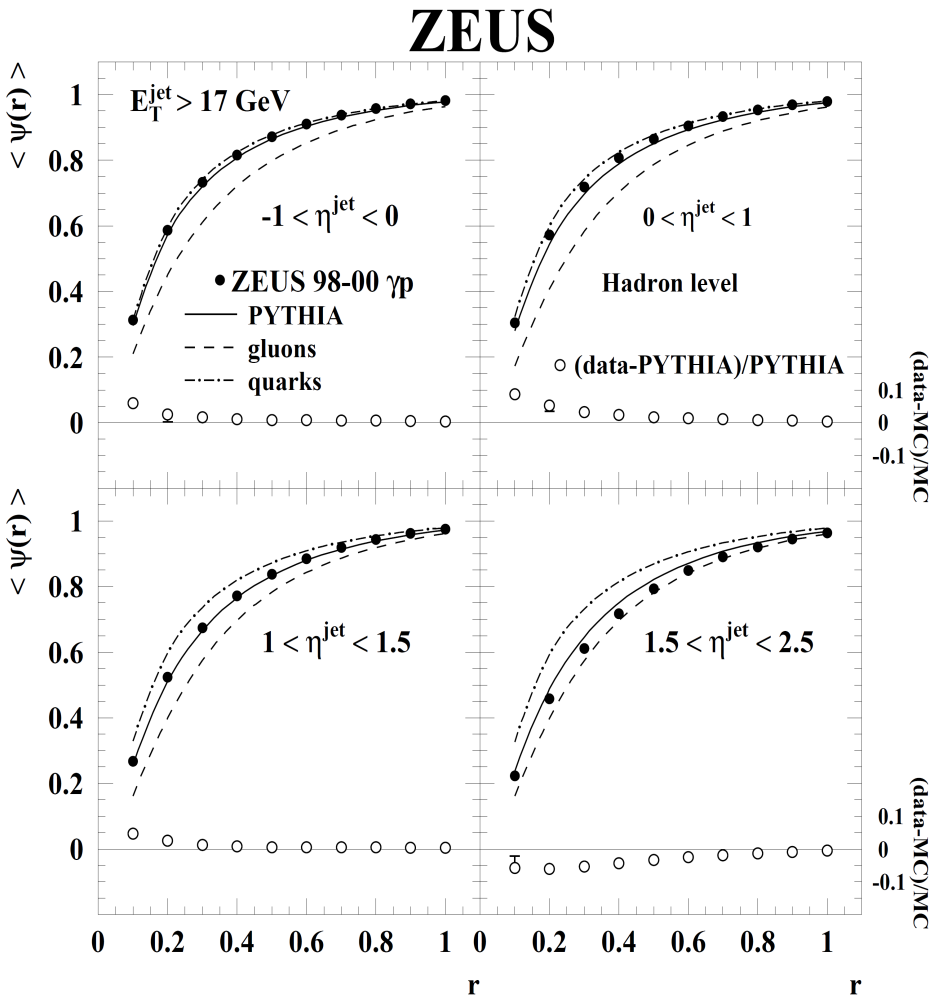

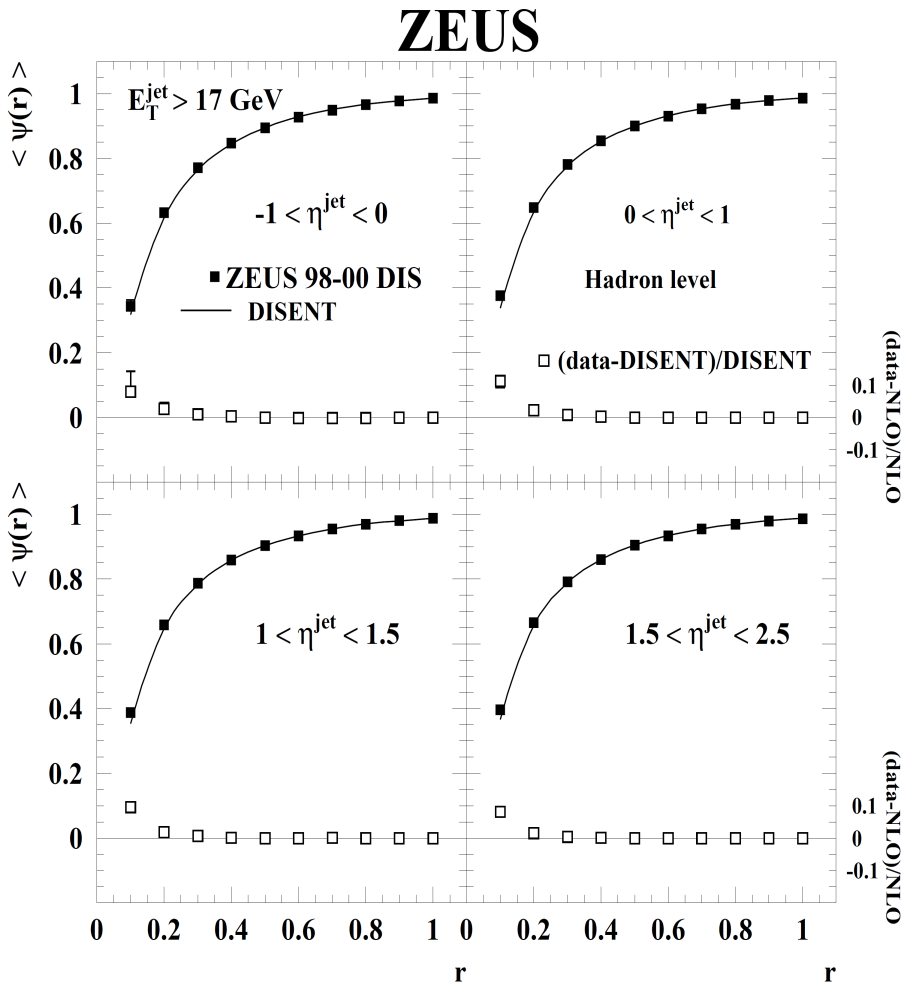

Global structure of hadronic events: Event shapes

Measure of how spherical is the distribution of hadrons in jet events.

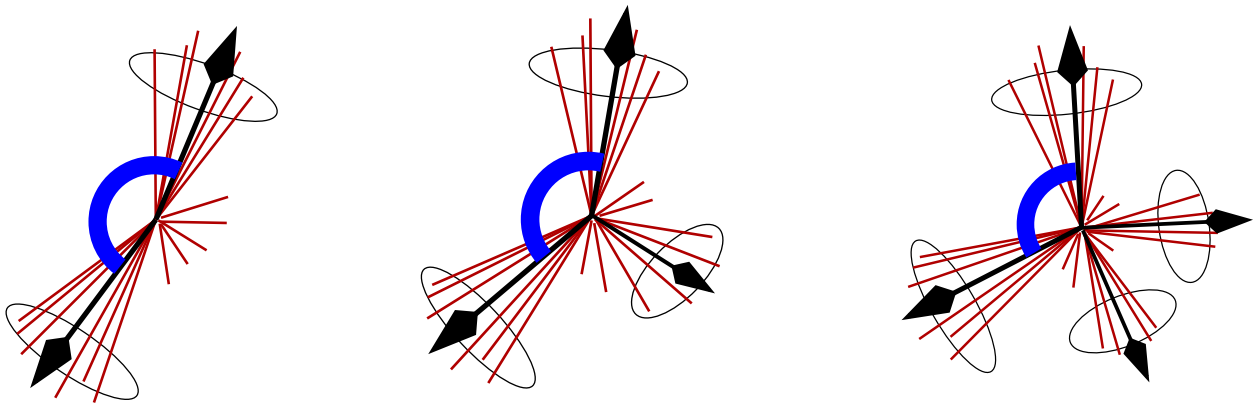

Classical examples are thrust and combinations of the eigenvalues of sphericity tensor ($\lambda_1 \geq \lambda_2 \geq \lambda_3$)

$$T = \max_{|\vec{n}|=1} \frac{\sum_i \vec{n} \cdot \vec{p}_i}{\sum_i |\vec{p}_i|}; \qquad S^{\alpha\beta} = \frac{\sum_i p_i^\alpha p_j^\beta}{\sum_i |\vec{p}_i|^2}$$

Sphericity and aplanarity:

$$S = \frac{3}{2}(\lambda_2 + \lambda_3); \quad A = \frac{3}{2}\lambda_3$$

Historical perspective: event shapes in e^+e^- annihilation

Precision test of QCD in e^+e^- annihilation

[ALEPH Collaboration, Eur. Phys. J. C 35 457 (2004)]

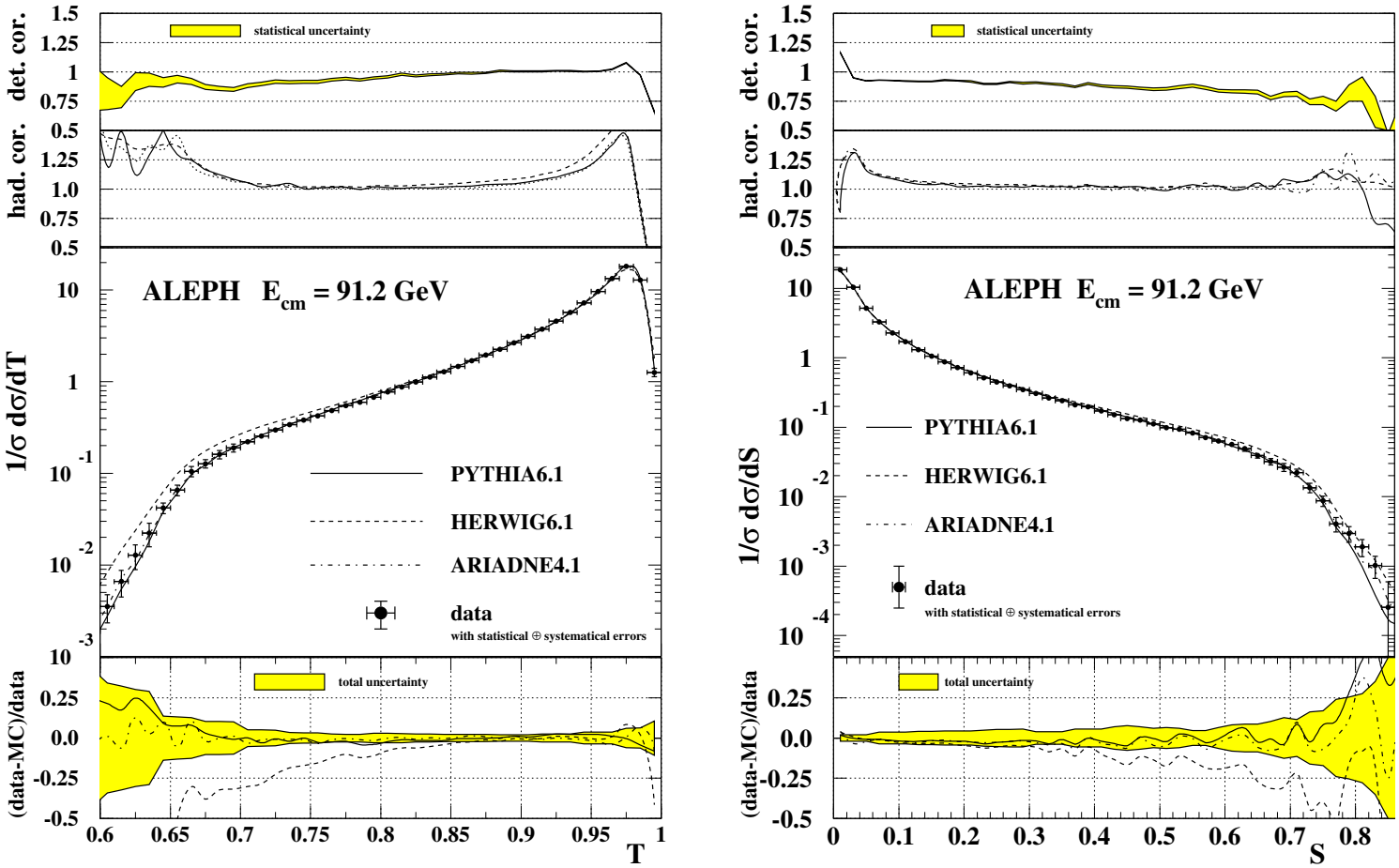

Recent α_s determinations

Recent determinations of the strong coupling by CMS from jet observables

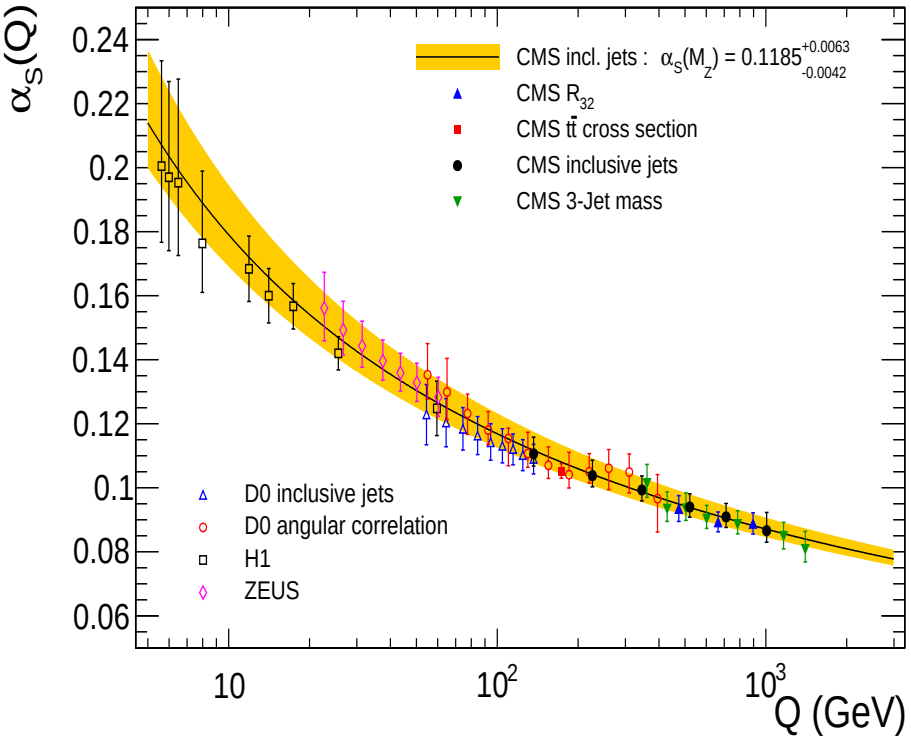

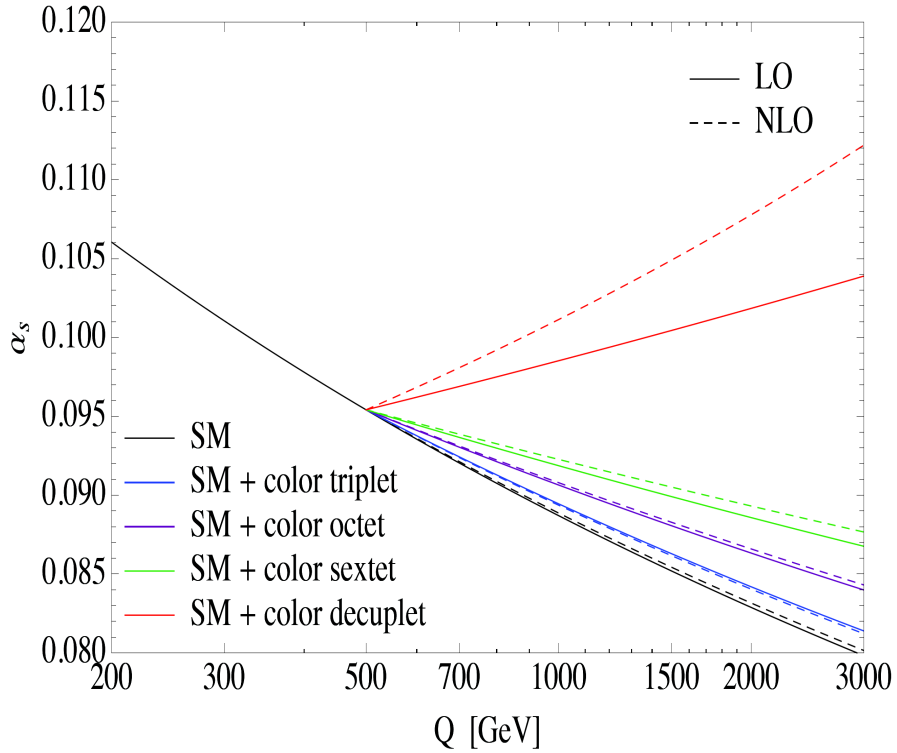

The study of the running of $\alpha_s(Q^2)$ can potentially be a hint for new physics (see talk by F. Sannino at α_s workshop at CERN (October 12 and 13, 2015)

II. The ATLAS detector and jet reconstruction.

The ATLAS detector

- Multi-purpose particle detector at the LHC
- Sampling calorimeters with high granularity (3 EM layers, 3 Had layers)
- High-efficiency jet reconstruction

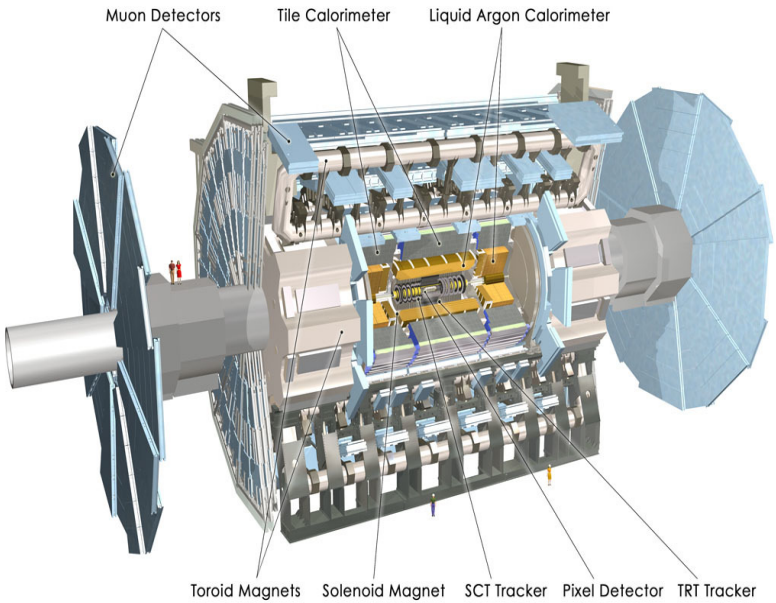

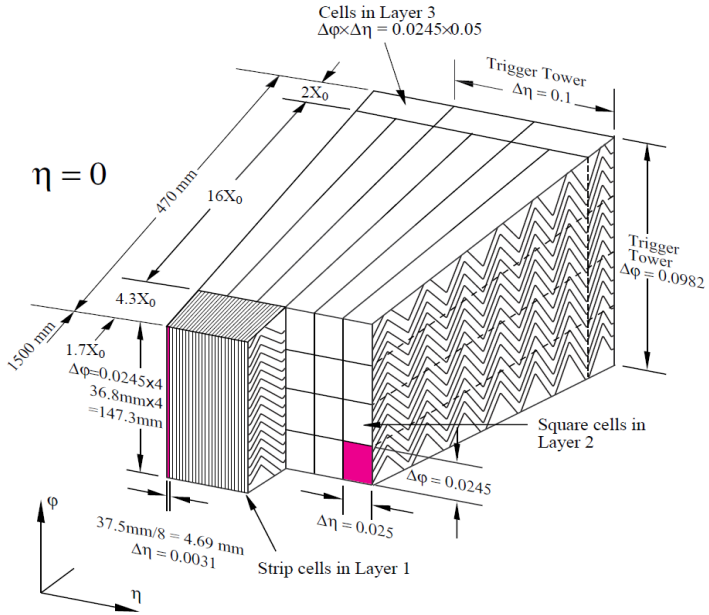

Jet reconstruction in ATLAS

Inputs to jet reconstruction: 3-Dimensional Topological Clusters.

- Iteratively constructed from calorimeter cells.
- Seeded from $|E| > 4\sigma$ cells. $|E| > 2\sigma$ cells and perimeter cells are added.
- Variable size.
- Aim to contain the shower from each hadron.

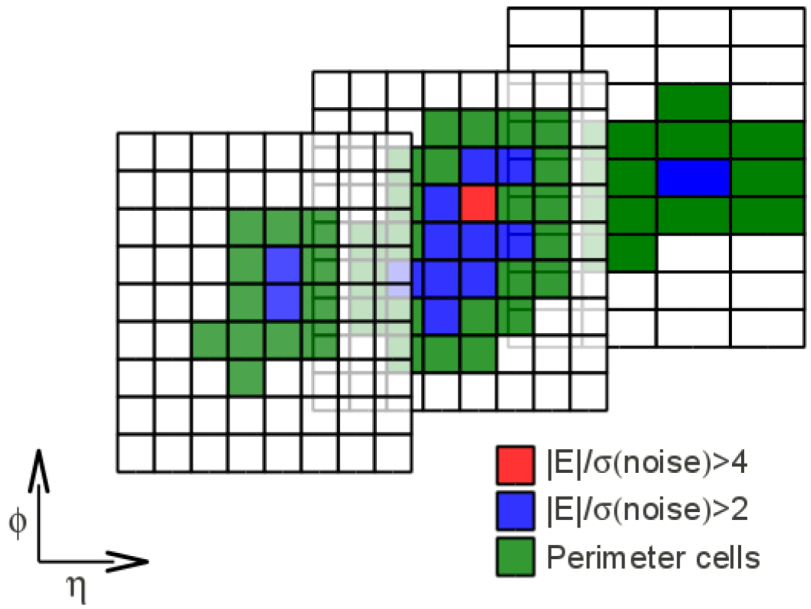

Jet algorithm: anti-k_T.

- Iterative algorithm based on the metric d_{ij}
- Infrared and collinear safe.
- Radius parameter $R = 0.4$.

$$\left.\begin{aligned} d_{ij} &= \min\left(\frac{1}{k_{Ti}^2}, \frac{1}{k_{Tj}^2}\right)\frac{\Delta R_{ij}^2}{R^2} \\ d_{iB} &= \frac{1}{k_{Ti}^2} \end{aligned}\right\}$$

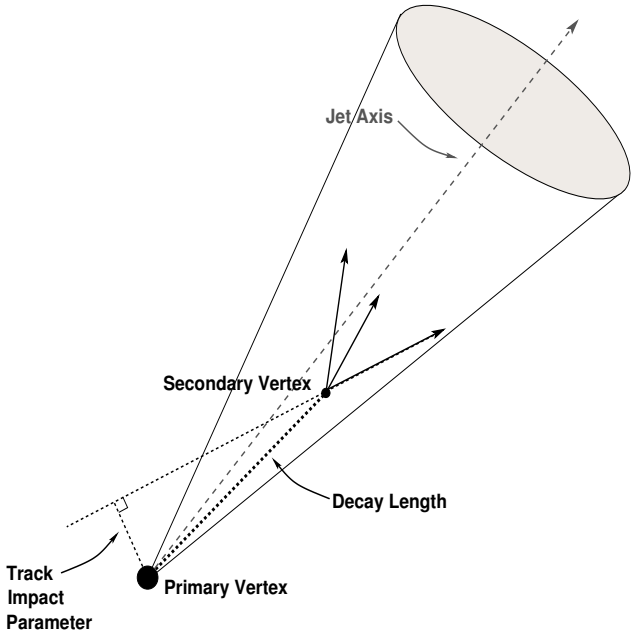

Main features

- Displaced vertex ($\tau_B \sim 1$ ps)
- Impact parameter significance d_0/σ_{d_0}
- Other: Vertex mass, Energy fraction...
- Use of NN algorithms to achieve better performance.

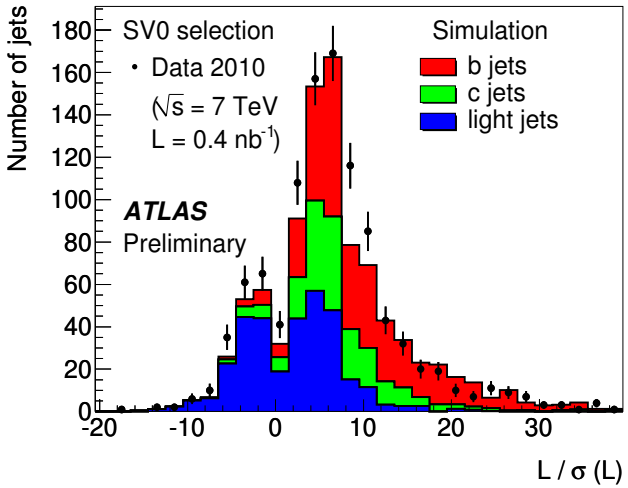

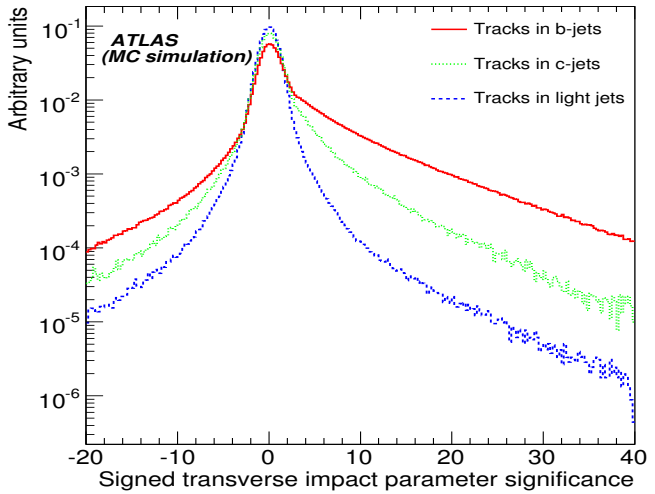

III. Measurement of jet shapes in $t\bar{t}$ events

The ATLAS Collaboration, Eur. Phys. J. **C73** 2676 (2013)

J. Llorente, F. Barreiro. ATL-COM-PHYS-2012-169

The dead cone effect (I)

The angular distribution of the radiation off a quark is modulated by its mass.

[G. Marchesini and B. R. Webber. Nucl. Phys. **B330** 261-283 (1990)]
[Yu L. Dokshitzer, V. A. Khoze and S. I. Troyan. J. Phys. **G17** 1602 (1991)]

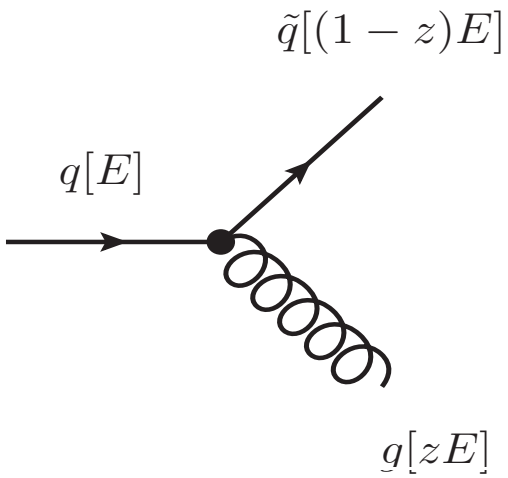

The opening angle is proportional to m_q

$$m_q^2 \simeq 2E_{\tilde{q}}E_g(1-\cos\theta) = E_{\tilde{q}}E_g\theta^2 + \mathcal{O}(\theta^4)$$

$$\theta \simeq \frac{m_q}{\sqrt{E_{\tilde{q}}E_g}} = \frac{1}{\sqrt{z(1-z)}}\frac{m_q}{E_q}$$

The probability of gluon emission at small angle θ depends on the ratio $\theta_0 = \frac{m_q}{E_q}$

$$\left(\frac{d\sigma}{d\omega}\right)_{q\to\tilde{q}g} = \frac{\alpha_s C_F}{\pi\omega}\frac{(2\sin\theta/2)^2 d(2\sin\theta/2)^2}{[(2\sin\theta/2)^2+\theta_0^2]^2}\left[1+\mathcal{O}(\theta_0,\omega)\right] \sim \frac{1}{\omega}\frac{\theta^2 d\theta^2}{[\theta^2+\theta_0^2]^2}$$

The amount of radiation is highly suppressed for $\theta < \theta_0$ (dead cone)

The dead cone effect (II)

The differential cross section $d\sigma/d\theta$ depends on both the quark mass m_q and the angle θ_{qg} between the quark and the radiated gluon

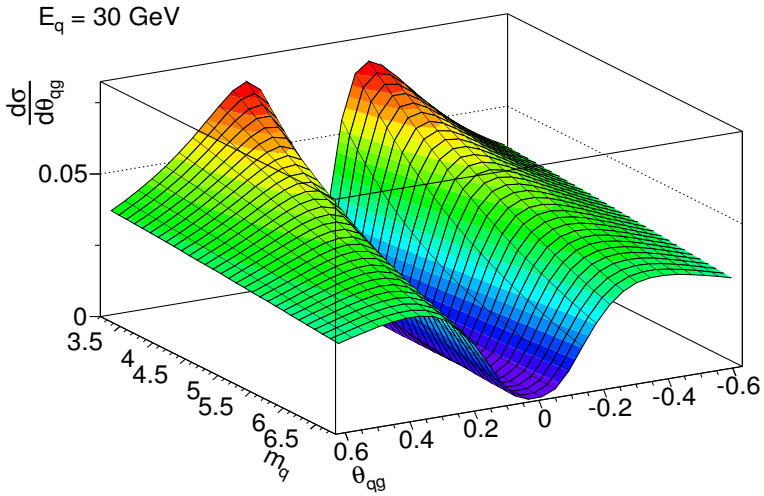

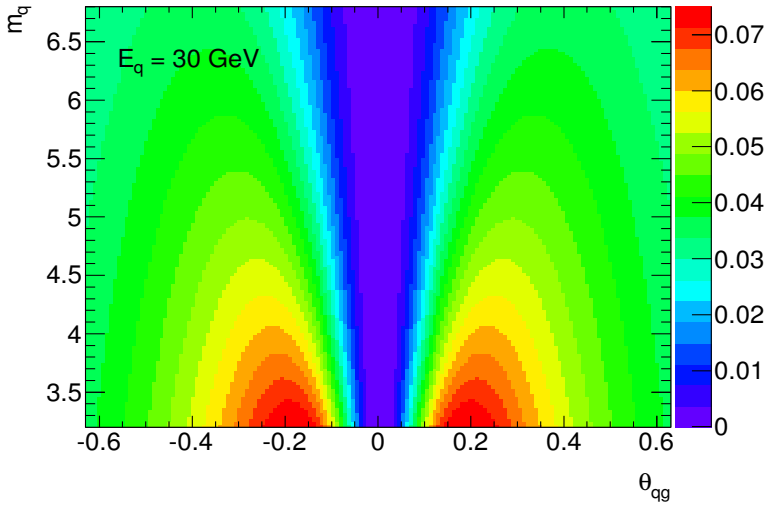

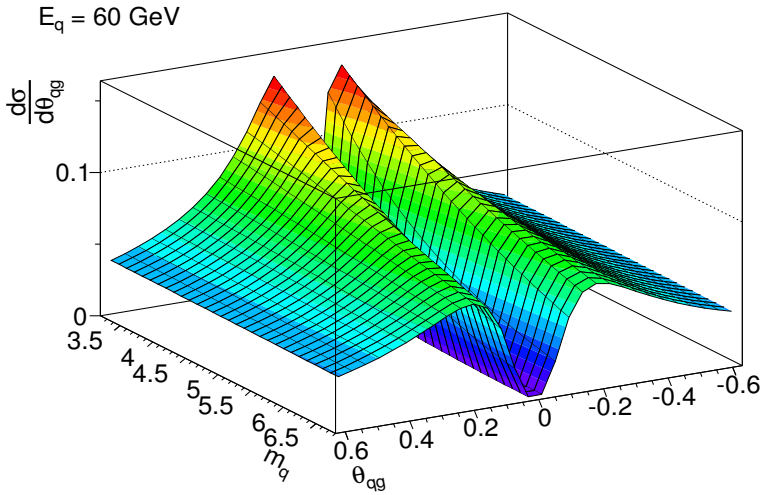

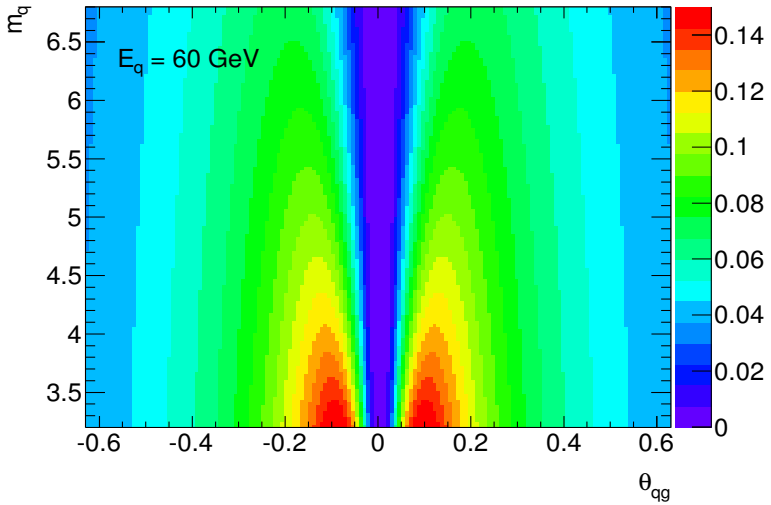

Event selection (Single-lepton channel)

- Trigger: Inclusive 20 GeV electron or 18 GeV muon.
- One isolated lepton with $E_T^e > 25$ GeV or $p_T^\mu > 20$ GeV.
- At least 4 jets with $p_T > 25$ GeV and $|\eta| < 2.5$.
- At least one b-tagged jet (efficiency $\epsilon_b = 57\%$).
- $E_T^{miss} > 35$ GeV (e-channel) or $E_T^{miss} > 20$ GeV (μ-channel)
- $m_T^W > 25$ GeV (e-channel) or $m_T^W + E_T^{miss} > 60$ GeV (μ-channel).

$$m_T^W = \sqrt{2 p_T^\ell E_T^{miss} (1 - \cos \Delta\phi_{\ell\nu})}$$

Process	Expected events	Fraction
$t\bar{t}$	14000 ± 700	77.4%
W + jets ($W \to \ell\nu$)	2310 ± 280	12.8%
Other EW (Z, diboson)	198 ± 18	1.1%
Single top	668 ± 14	3.7%
Multi-jet	900 ± 450	5.0%
Total Expected	18000 ± 900	
Total Observed	17019	

Event selection (Dileptonic channel)

- Two isolated leptons with $E_T^e > 25$ GeV or $p_T^\mu > 20$ GeV.
- At least two jets with $p_T > 25$ GeV and $|\eta| < 2.5$.
- Missing energy $E_T^{miss} > 60$ GeV (ee,$\mu\mu$) and $H_T > 130$ GeV ($e\mu$).
- Dilepton invariant mass $m_{\ell\ell} > 15$ GeV and $|m_{\ell\ell} - m_Z| \geq 10$ GeV.
- At least one b-tagged jet ($\epsilon_b = 57\%$).

Process	Expected events	Fraction
$t\bar{t}$	2100 ± 110	94.9%
Z + jets ($Z \to \ell^+\ell^-$)	14 ± 1	0.6%
Other EW (W, diboson)	4 ± 2	0.2%
Single top	95 ± 2	4.3%
Multi-jet	0^{+2}_{-0}	0.0%
Total Expected	2210 ± 110	
Total Observed	2067	

Top quark pair event displays I (Atlantis)

A semileptonic $t\bar{t}$ event with $W \to \mu\nu_\mu$, recorded during the 2011 pp run is displayed below

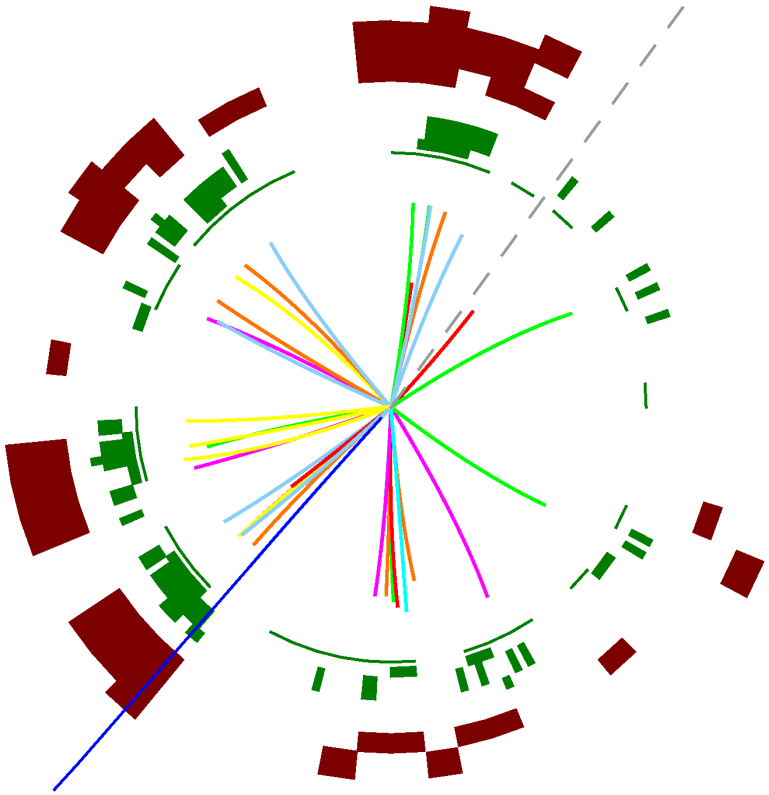

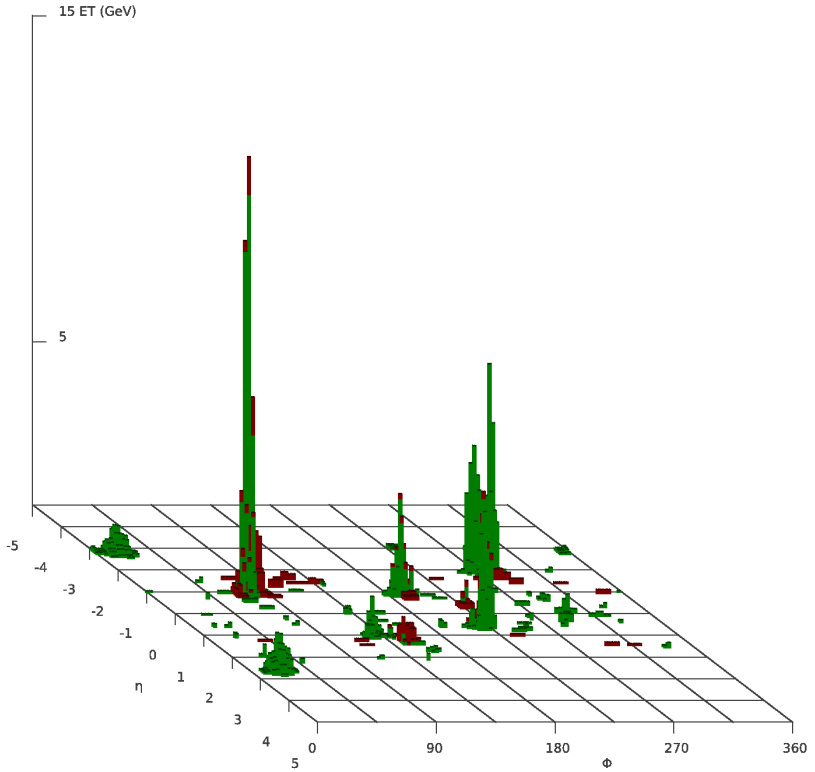

Top quark pair event displays II (Atlantis)

A dileptonic $t\bar{t}$ event with $W^{\pm} \rightarrow e^{\pm}\nu_e$, recorded during the 2011 pp run is displayed below

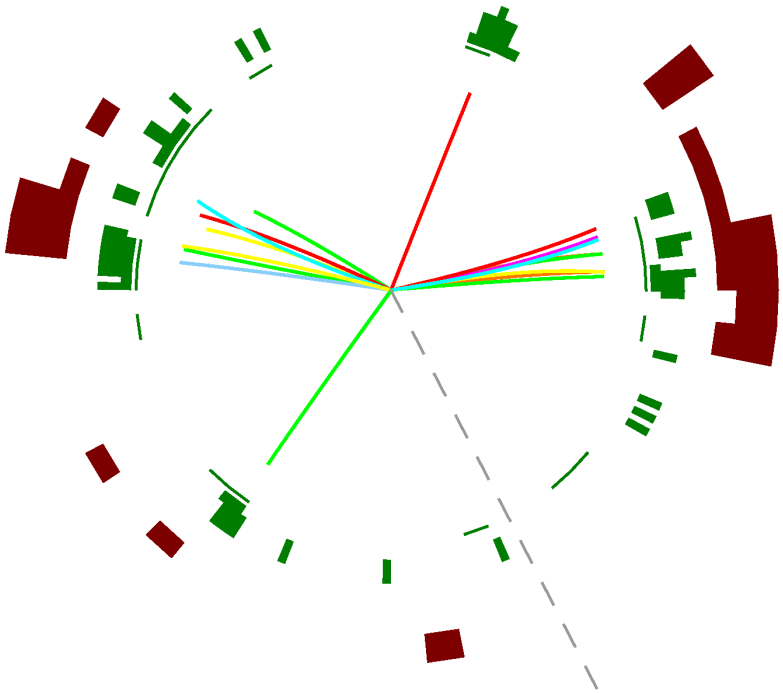

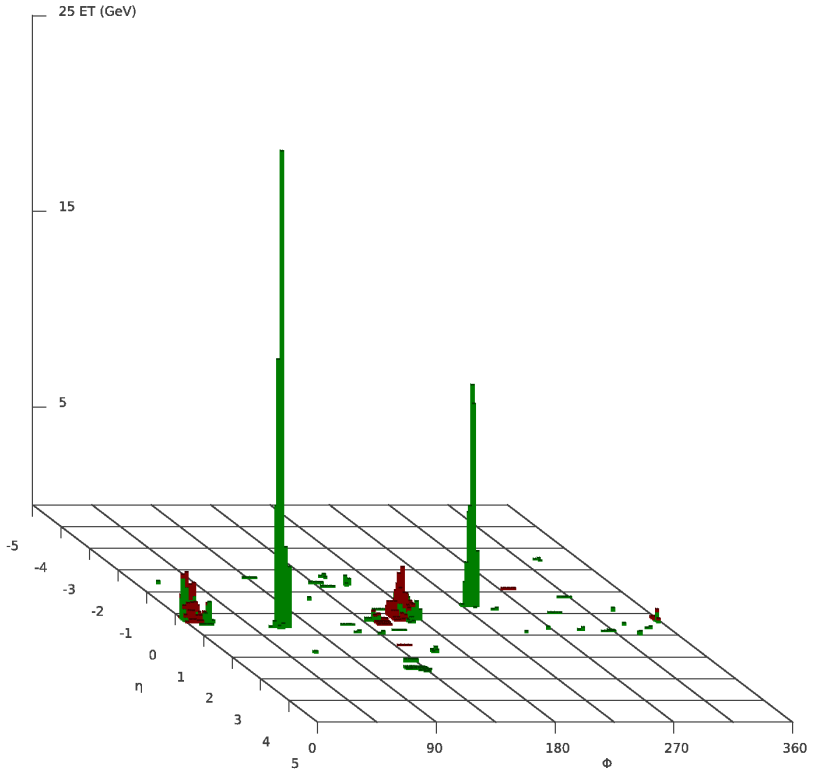

b-jet selection

Two samples of *b*-jets are selected in the semileptonic and dileptonic decay modes, with the following selection criteria

- *b*-tagged with $\epsilon_b = 57\%$.
- $\Delta R_{bj} > 0.8$ (isolated jets).
- $|JVF| > 0.75$ to avoid pileup jets.

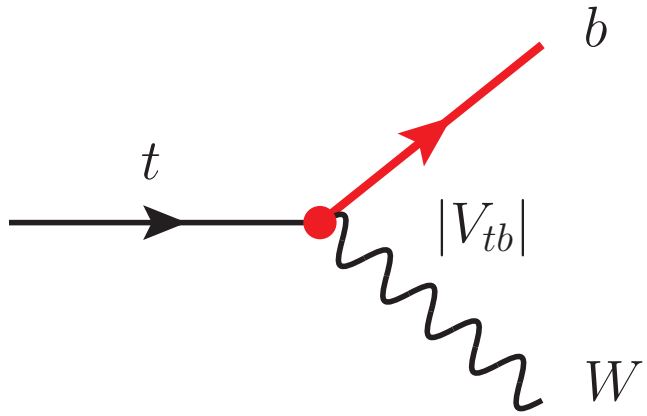

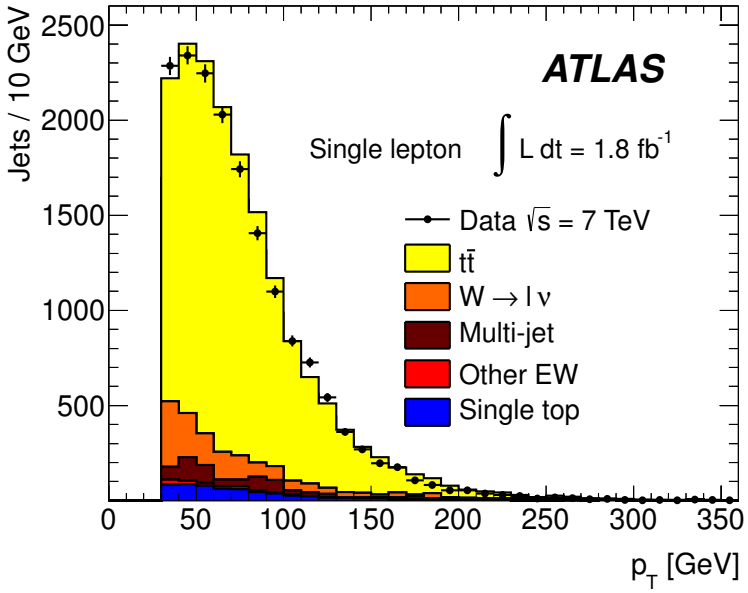

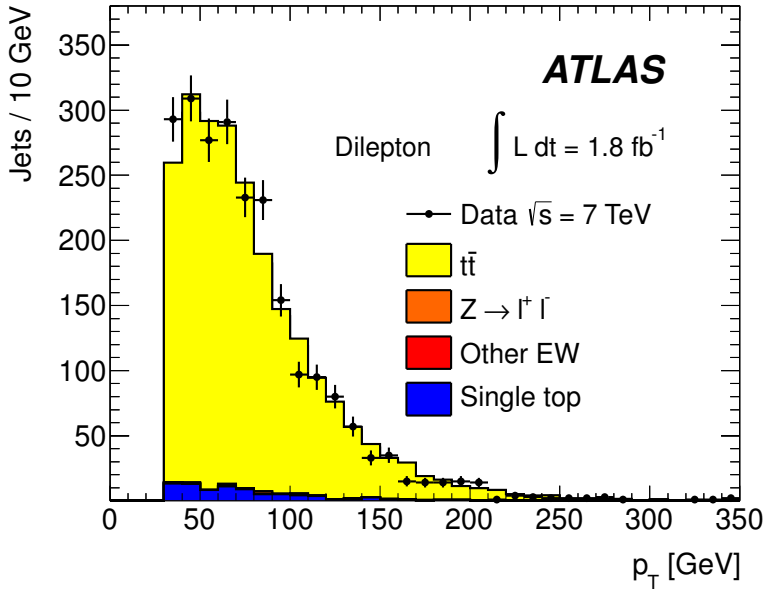

Light jet selection

The light jet sample is selected from the $W \to q\bar{q}'$ decays in the semileptonic decay channel with the following criteria

- Pair with closest mass to m_W.
- Anti b-tagged with $\epsilon_b = 57\%$.
- $\Delta R_{lj} > 0.8$ (isolated jets).
- $|JVF| > 0.75$ to avoid pileup jets.

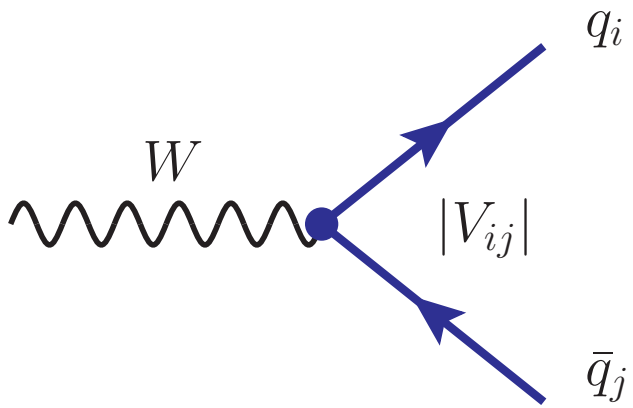

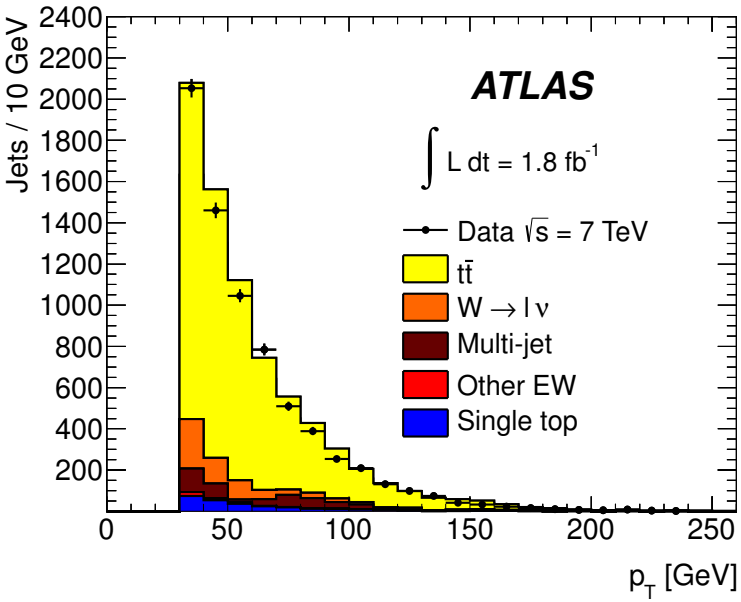

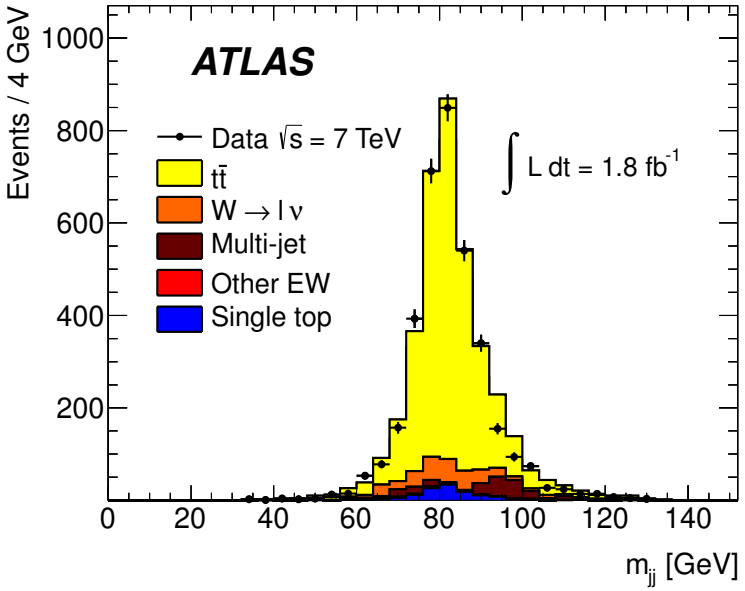

Purity

The purities of the jet samples are estimated taking into account the partial purities in the signal and background processes

$$p = \sum_k \alpha_k p_k; \quad p_k = 1 - \frac{N_{\mathrm{f}}^{(k)}}{N_{\mathrm{T}}^{(k)}}$$

The results for both samples of b-jets and the light jet sample are

- b-jet purity ($\ell q\bar{q}'$): $p_b = (88.5 \pm 5.7)\%$
- b-jet purity ($\ell\ell$): $p_b = (99.3^{+0.7}_{-6.5})\%$
- Light jet purity ($\ell q\bar{q}'$): $p_l = (66.2 \pm 4.1)\%$

Average values $\langle \rho(r) \rangle$ and $\langle \Psi(r) \rangle$ at the detector level.

Left figure shows the detector-level differential jet shapes once binned in p_T and averaged over jets. On the right, the analogous for the integrated jet shapes.

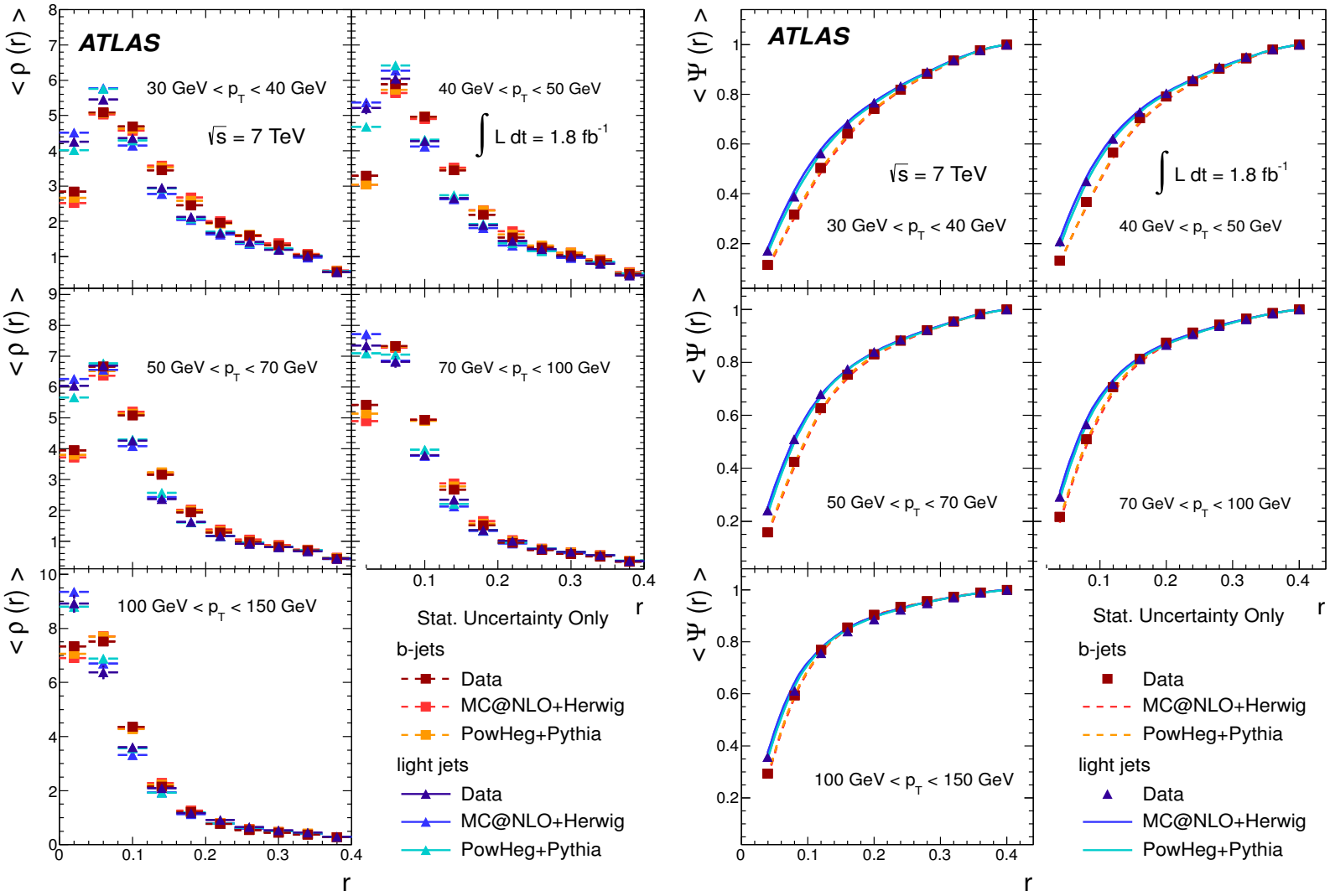

Dependence with jet kinematics

Jet shapes are found to be very dependent with jet transverse momentum p_T and mildly dependent on pseudorapidity for both light and b-jets.

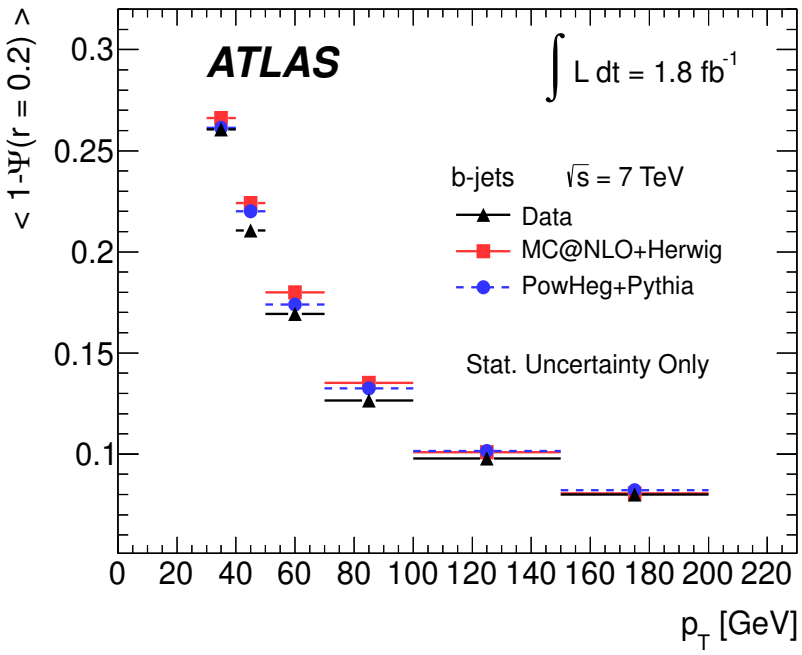

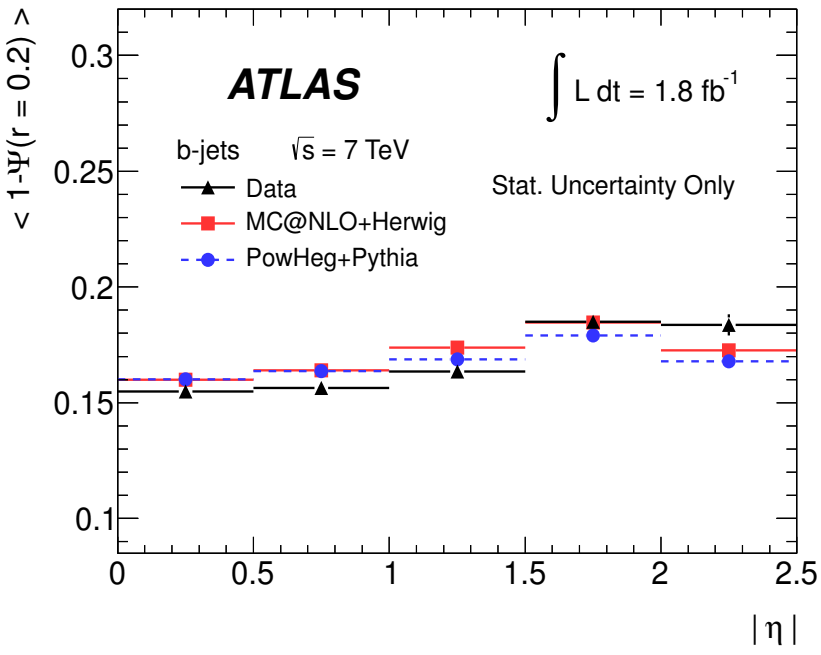

Particle jet defintion

All particle jets fulfill the same kinematic requirements than reconstructed jets: $p_T > 25$ GeV, $|\eta| < 2.5$ and $\Delta R_{jj} > 0.8$.

- Particle jets: anti-k_T jets for particles with average lifetime $\tau > 10^{-11}$ s, excluding muons and neutrinos.
- Particle b-jet: A particle jet containing a B-hadron closer than $\Delta R_{Bj} = 0.3$ to the jet axis.
- Particle light-jets: Pair of non-b particle jets with closest invariant mass to m_W.

Correction factors

Bin-by-bin factors are calculated for the average values $\langle \rho(r) \rangle$ and $\langle \Psi(r) \rangle$.

$$F^{\rho}_{l,b}(r) = \frac{\langle \rho(r)_{l,b} \rangle_{\mathrm{MC,part}}}{\langle \rho(r)_{l,b} \rangle_{\mathrm{MC,det}}}; \qquad F^{\Psi}_{l,b}(r) = \frac{\langle \Psi(r)_{l,b} \rangle_{\mathrm{MC,part}}}{\langle \Psi(r)_{l,b} \rangle_{\mathrm{MC,det}}}$$

Systematic uncertainties

For each bin (p_T,r) the total uncertainty is calculated as

$$\Delta\rho = \sqrt{(\Delta_{stat}\rho)^2 + \sum_{i=1}^{n} (\Delta_i\rho)^2}$$

Source i	Description	Impact $\Delta_i\rho/\rho$
Cluster Systematics	Energy Scale, Angular Resolution	$2\% - 10\%$
Pileup	Number of primary vertices	$2\% - 10\%$
Unfolding-Model	Parton shower modelling	$1\% - 8\%$
Jet Energy Scale	Uncertainty on the jet calibration	$\simeq 5\%$
Jet Energy Resolution	Calorimeter energy resolution σ	$\simeq 5\%$
JVF	JVF-related uncertainty	$< 1\%$
	Total uncertainty	$10\% - 15\%$

All numbers are publicly available in

http://hepdata.cedar.ac.uk/view/ins1243871

Unfolded results: 30 GeV $< p_T <$ 40 GeV

Differential $\langle \rho(r) \rangle$

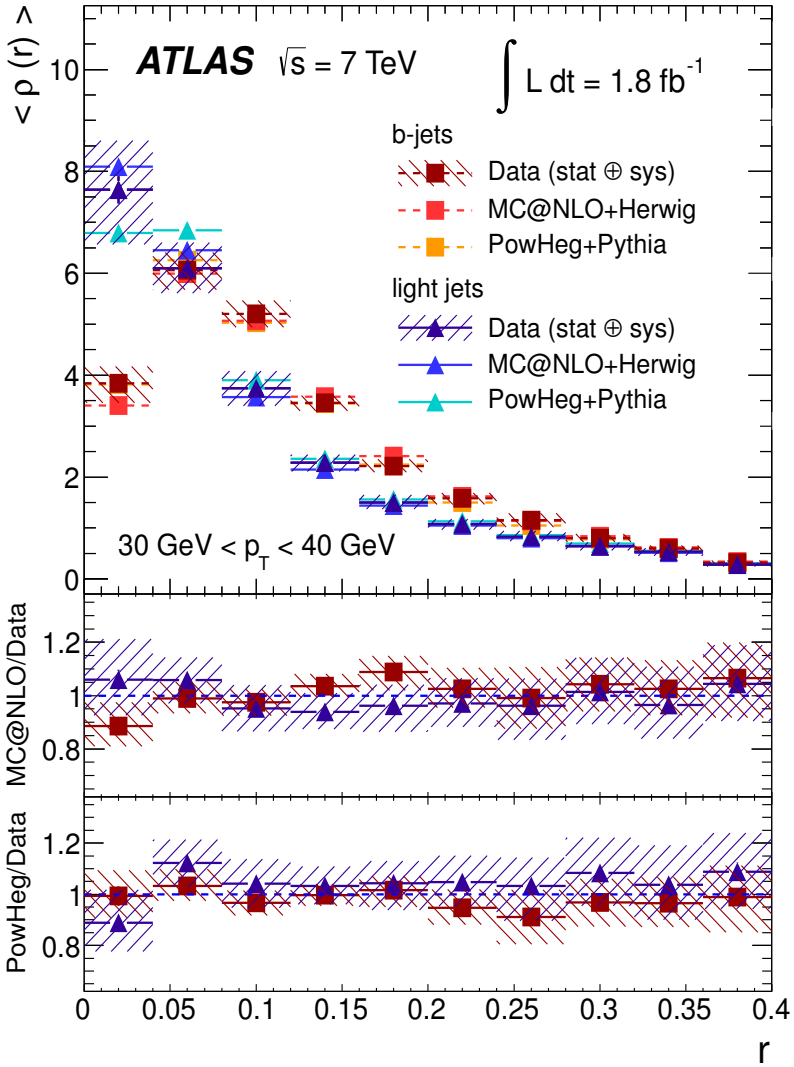

Integrated $\langle \Psi(r) \rangle$

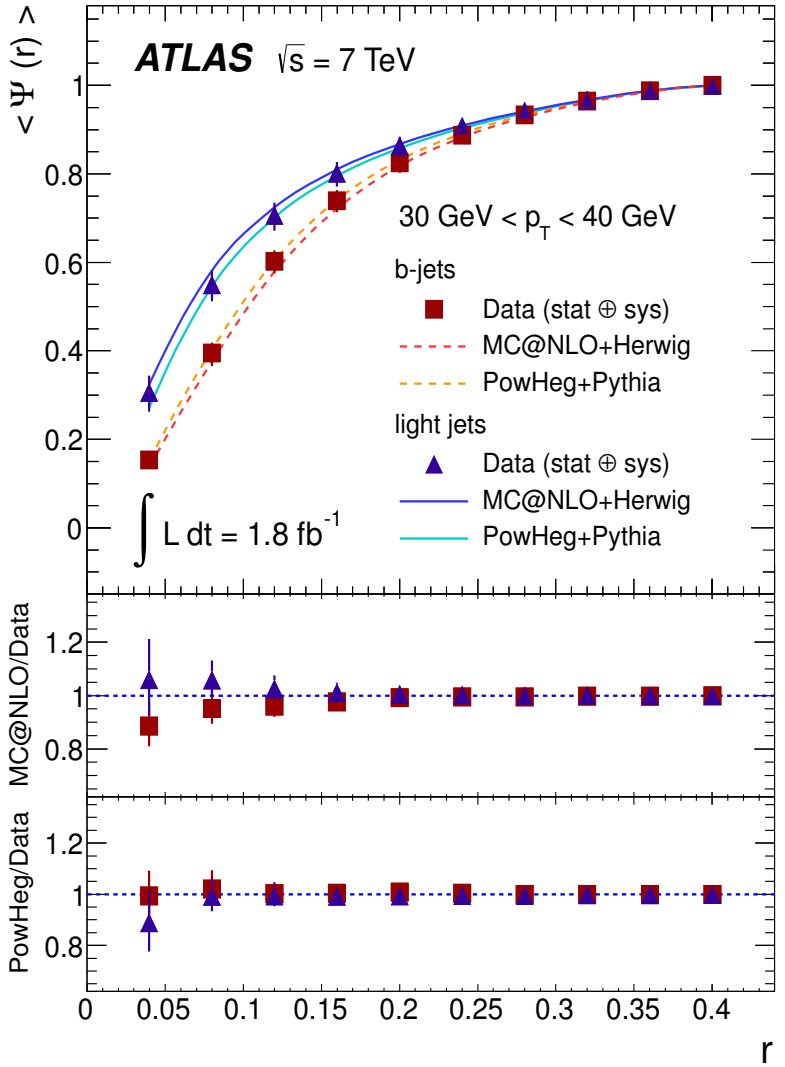

Unfolded results: 40 GeV $< p_T <$ 50 GeV

Differential $\langle \rho(r) \rangle$

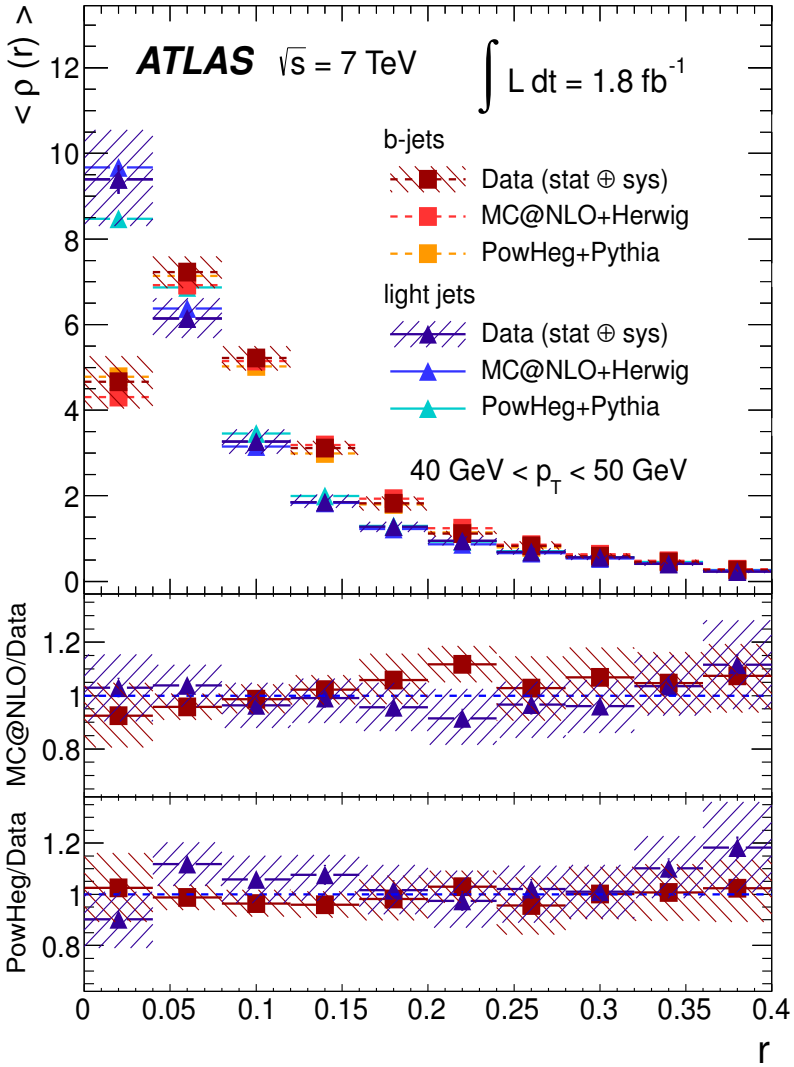

Integrated $\langle \Psi(r) \rangle$

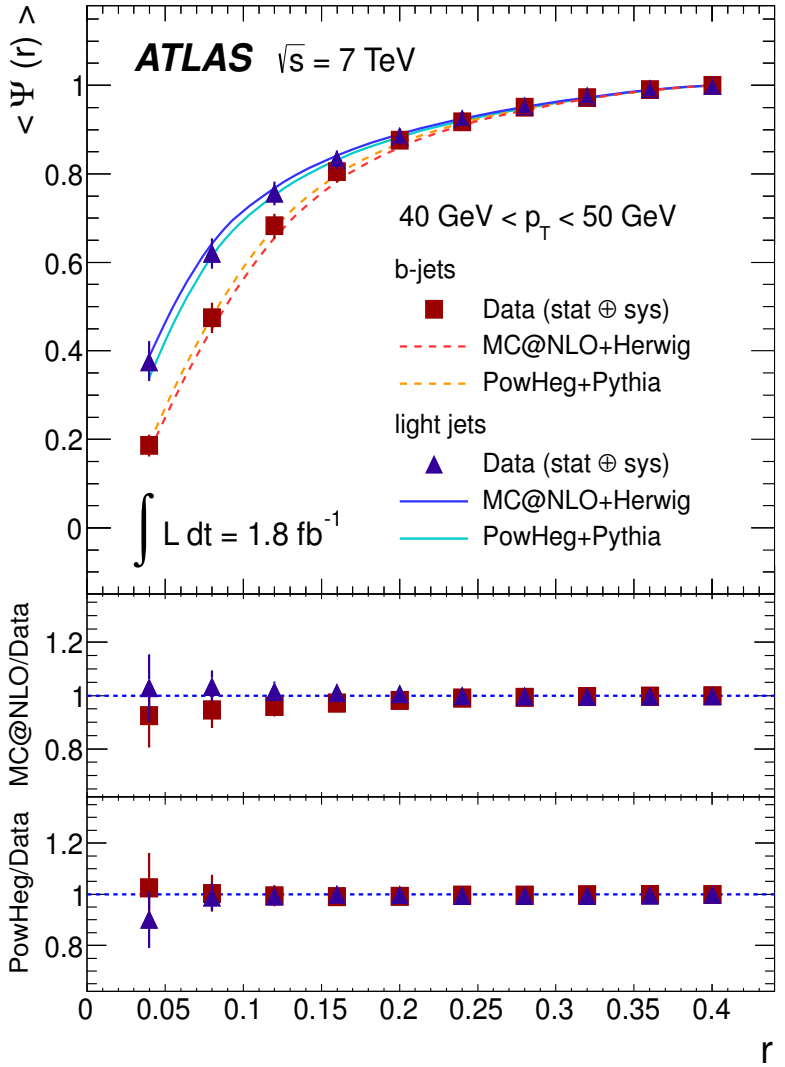

Unfolded results: 50 GeV $< p_T <$ 70 GeV

Differential $\langle \rho(r) \rangle$

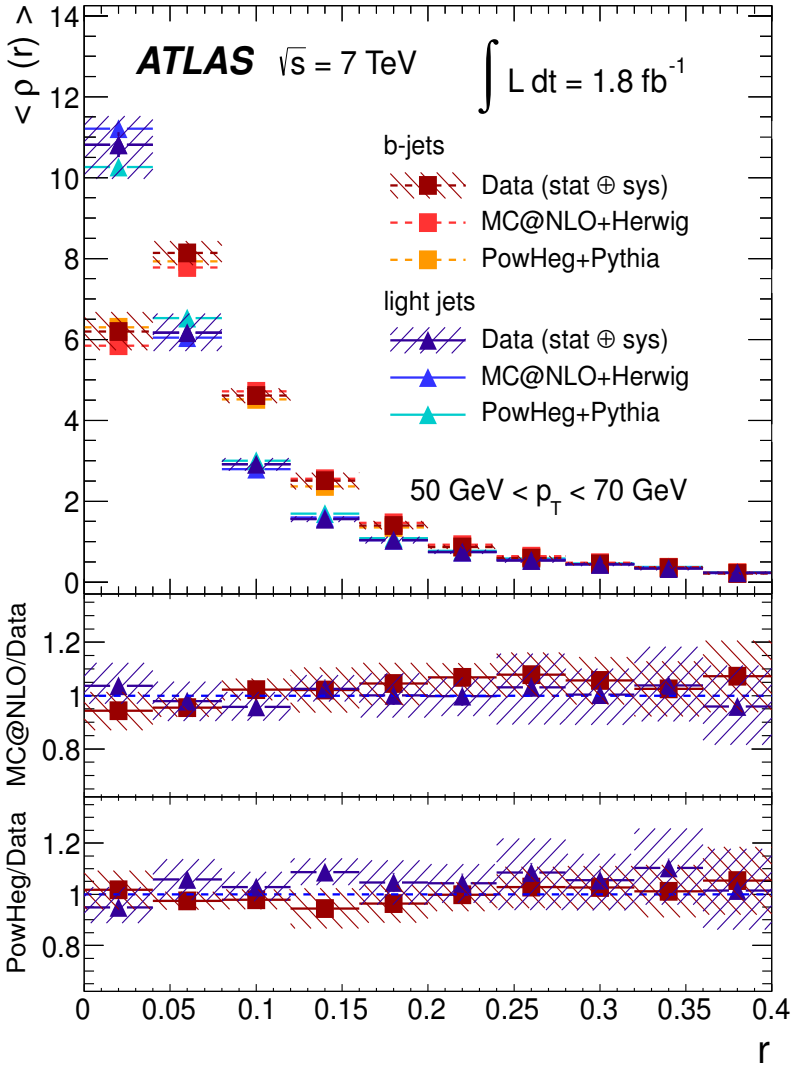

Integrated $\langle \Psi(r) \rangle$

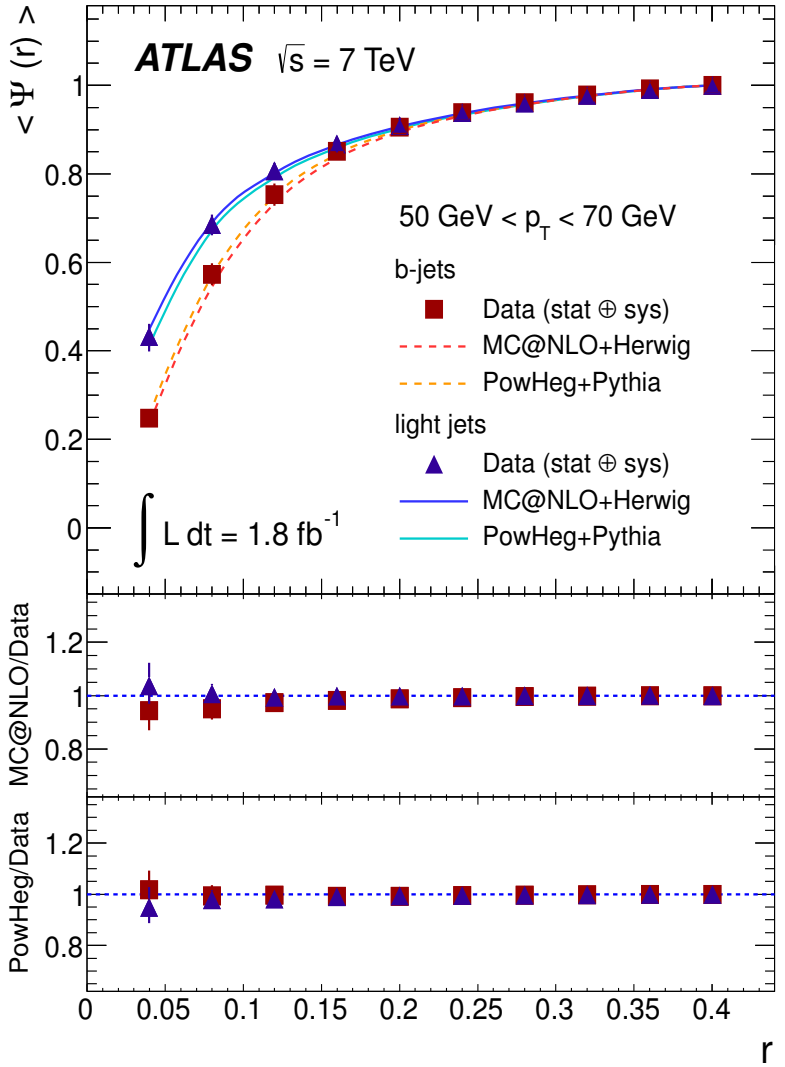

IV. Determination of the bottom quark mass

J. Llorente and J. Cantero, Nucl. Phys. **B889** 401-418 (2014)

Determination of the b-quark mass

Bottom quark jets are wider because of the heavier mass of the b-quark, but is it possible to extract the b-quark mass from these data?

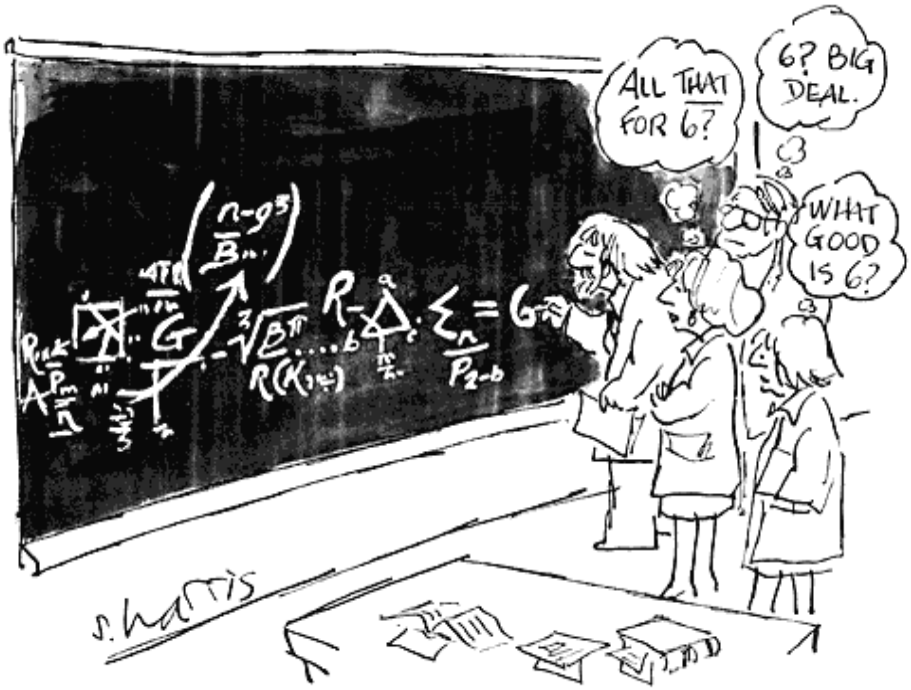

- b-jet shapes depend on both the strong coupling α_s and the b mass.
- Light jet shapes depend only on α_s via the QCD scale Λ
- The simultaneous determination of both parameters is not possible. There is a full set of degenerate minima in the (Λ_s, m_b) plane.

Strategy: Extract Λ_s from light jet data and use it for fitting m_b from b-jets.

Parameter extraction: χ^2 definition

The determination of a physical parameter β from a distribution $\{x_k\}$ relies on the minimization of a χ^2 function.

$$\chi^2(\beta;\vec{\lambda}) = \sum_k \frac{(x_k - F_k(\beta;\vec{\lambda}))^2}{\Delta x_k^2 + \Delta \tau_k^2} + \sum_i \lambda_i^2$$

$$F_k(\beta;\vec{\lambda}) = \phi_k(\beta)\left(1 + \sum_i \lambda_i \sigma_{ik}\right)$$

- This method requires an analytical expression for the dependence of the observable on the parameter, given by $\phi_k(\beta)$.
- The correlations between sources of systematic uncertainty are accounted for using the nuisance parameters $\{\lambda_i\}$.
- Statistical uncertainty on the theoretical predictions also taken into account in $\Delta\tau_k$.

Dependence on the parton shower scale Λ_s (light jets)

Jet shapes depend on the strong coupling via Λ_s. This dependence has been evaluated using PYTHIA 6.4 + TUNE A, considering the LO running of α_s.

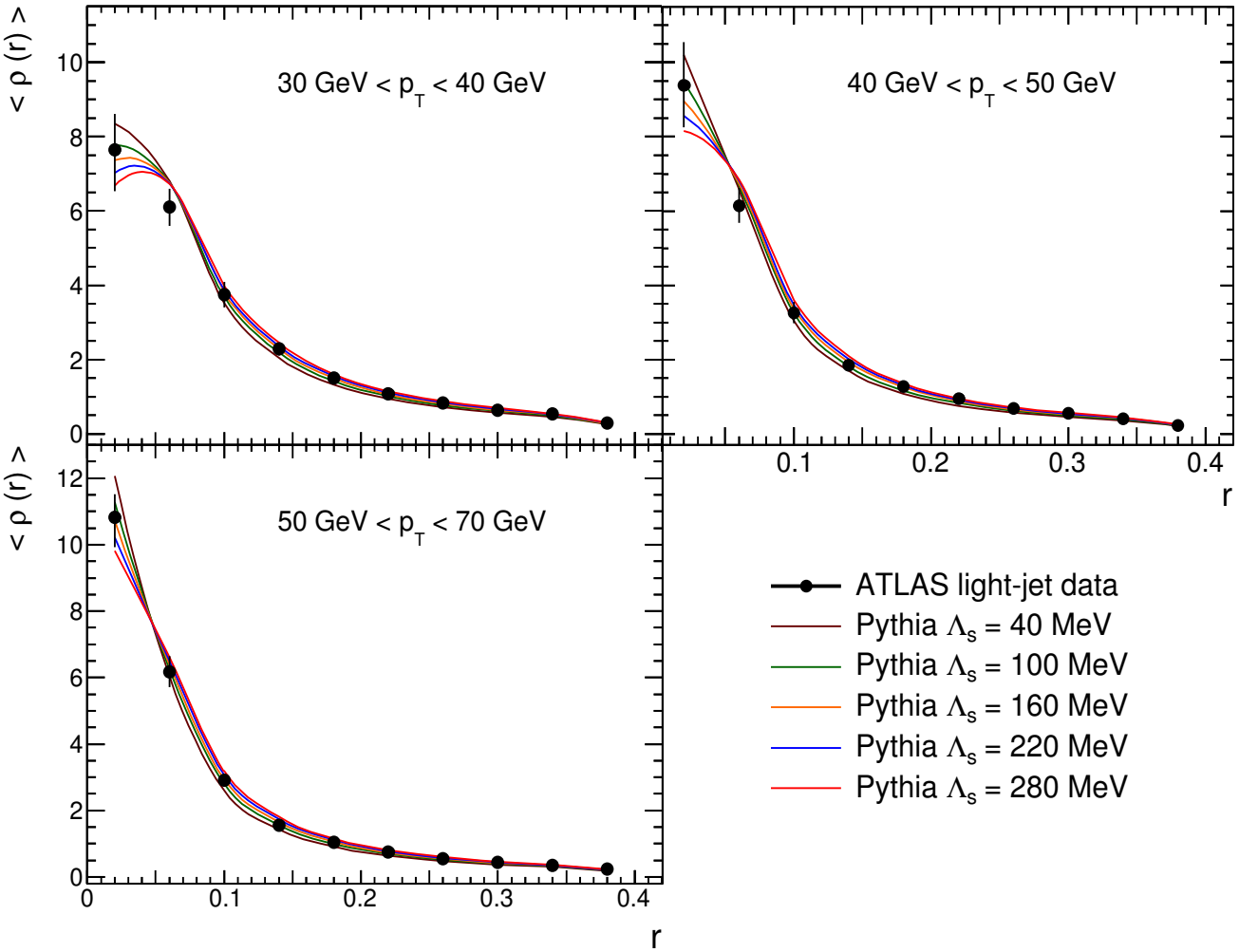

The interpolating functions $\phi_k(\Lambda_s)$

The analytical dependence of $\langle \rho(r) \rangle$ on Λ_s is obtained by fitting the Monte Carlo predictions to a second-order polynomial in each bin (p_T, r).

$$\phi_k(\Lambda_s) = a_k \Lambda_s^2 + b_k \Lambda_s + c_k$$

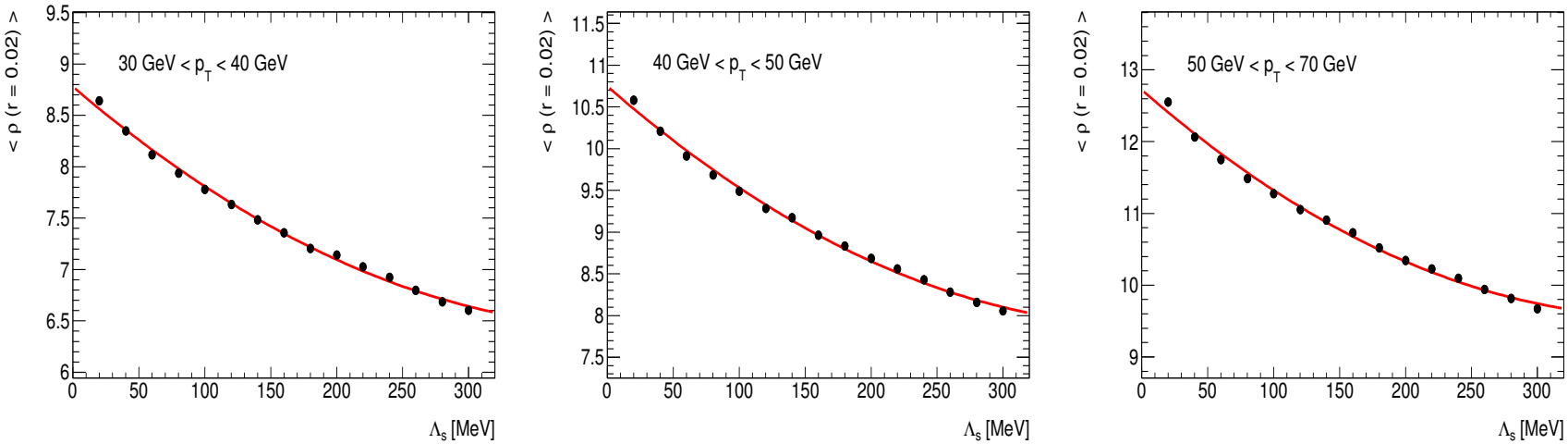

The PYTHIA time-like showers are evolved using the LO solution to the RGE

$$\alpha_s(Q^2) = \frac{1}{\beta_0 \log\left(\frac{Q^2}{\Lambda^2}\right)}; \quad \beta_0 = \frac{1}{4\pi}\left(11 - \frac{2}{3} n_f\right)$$

Results for Λ_s

The results on the value of Λ_s for each p_T bin studied are summarised in the following table

Bin	Λ_s value (MeV)	Fit error (MeV)	χ^2/N_{dof}
30 GeV $< p_T <$ 40 GeV	187.5	24.0	10.6 / 9
40 GeV $< p_T <$ 50 GeV	193.5	24.2	11.0 / 9
50 GeV $< p_T <$ 70 GeV	137.7	17.3	7.8 / 9
Global fit	162.1	9.6	39.0 / 29

Checks have been performed using HERWIG++:

- Using the LO solution to the RGE leads to $\Lambda_s = 160.7 \pm 15.3$ MeV. ✓
- For the NLO solution, the result is $\Lambda_s = 276.1 \pm 17.3$ MeV.

$$\alpha_s\left(x = \frac{Q^2}{\Lambda^2}\right) = \frac{1}{\beta_0 \log x}\left[1 - \frac{\beta_1}{\beta_0^2}\frac{\log(\log x)}{\log x}\right]; \quad \beta_1 = \frac{1}{(4\pi)^2}\left(102 - \frac{38}{3}n_f\right)$$

Dependence on the b-quark mass m_b (b-jets)

Jet shapes for b-quark jets depend also on m_b. The dependence is evaluated using PYTHIA 6.4 + TUNE A, using the previously extracted value of Λ_s

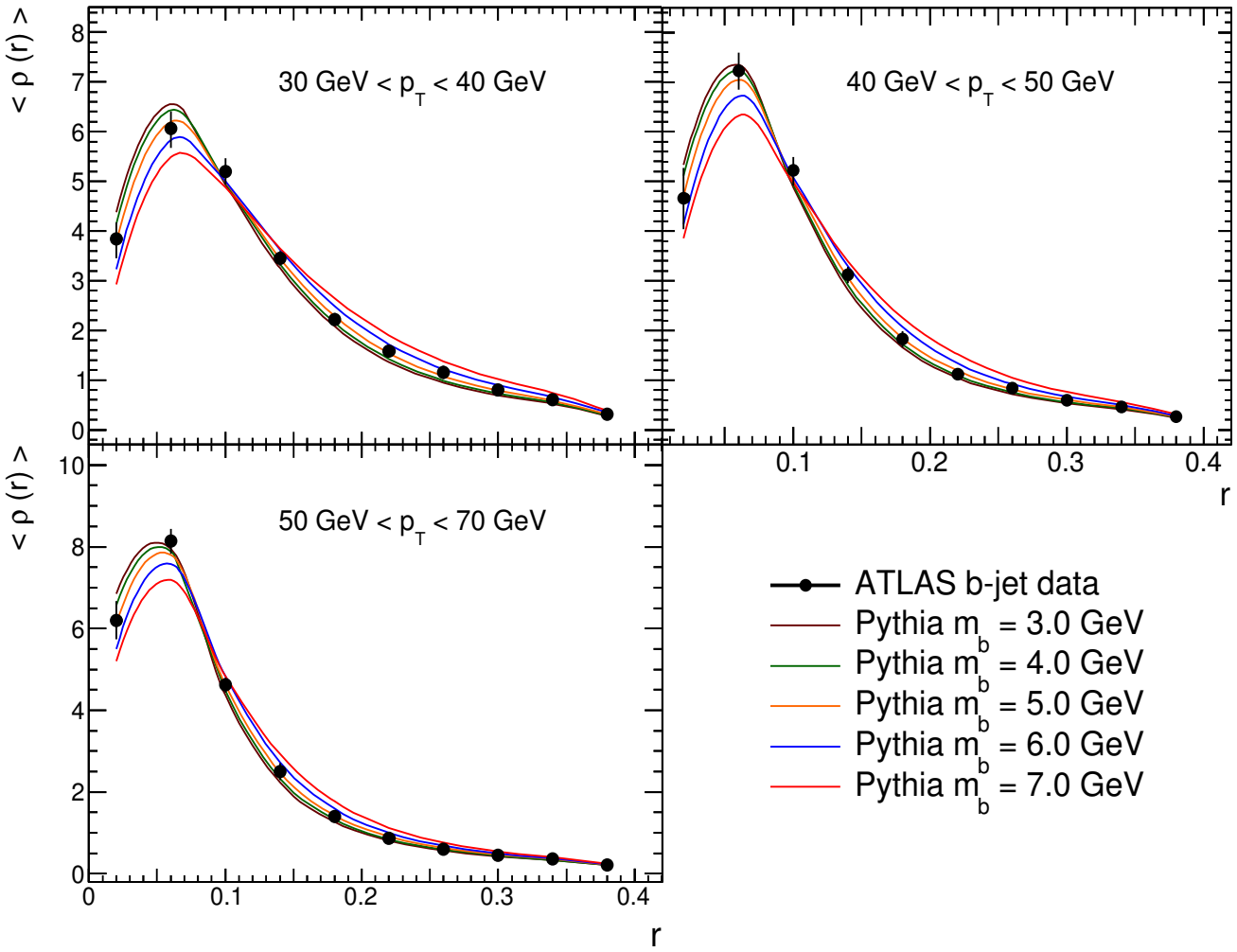

The interpolating functions $\phi_k(m_b)$

The analytical dependence of $\langle \rho(r) \rangle$ on m_b is obtained by fitting the Monte Carlo predictions to a second-order polynomial in each bin (p_T, r).

$$\phi_k(m_b) = a_k m_b^2 + b_k m_b + c_k$$

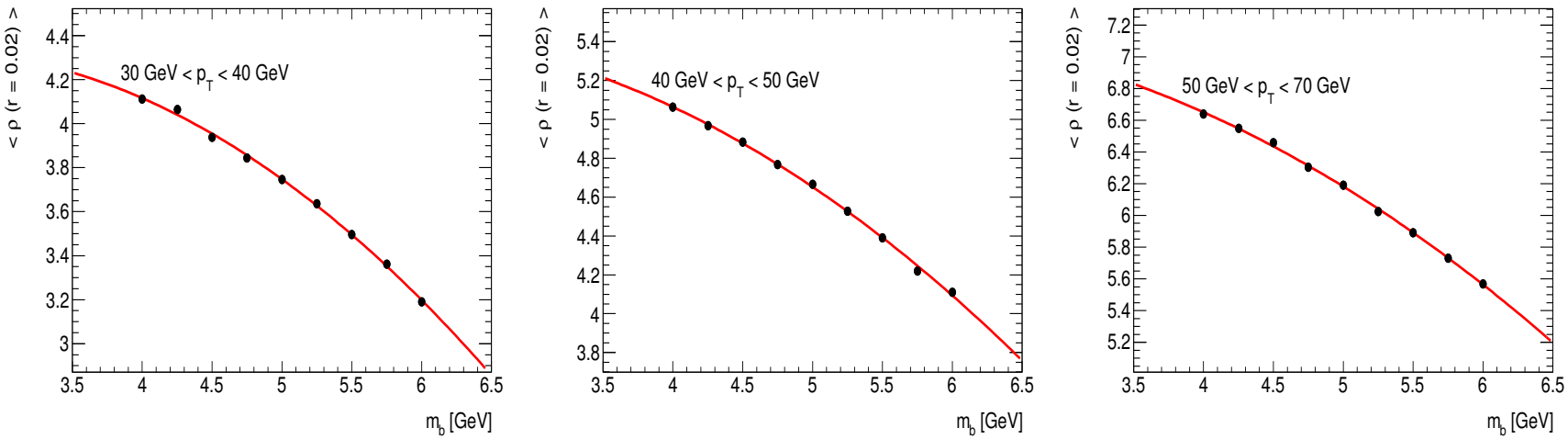

Results for m_b

The results on the value of m_b for each p_T bin studied are summarised in the following table. Each bin is fitted using its corresponding value of Λ_s, while the global fit is performed using the global value of Λ_s.

Bin	m_b value (GeV)	Fit error (GeV)	χ^2/N_{dof}
30 GeV $< p_T <$ 40 GeV	5.00	0.14	8.28 / 9
40 GeV $< p_T <$ 50 GeV	4.82	0.19	10.41 / 9
50 GeV $< p_T <$ 70 GeV	4.82	0.13	11.99 / 9
Global fit	4.86	0.08	43.04 / 29

Theoretical uncertainties

The theoretical uncertainties on the bottom mass are summarised below

- Generator modelling ($\sim 8\%$): The fits are repeated using HERWIG++.
- Initial / Final State Radiation ($\sim 4\%$): The PYTHIA parameters controlling ISR/FSR are varied up and down.
- Colour reconnection ($\sim 3.5\%$): An alternative model with stronger colour reconnection within Tune A is used.
- Uncertainty on the parton shower scale ($\sim 3\%$). Two sources of uncertainty:
  - The value of Λ_s is varied up and down by its uncertainty.
  - The 2-loop solution to the RGE is used to extract the value of m_b in HERWIG++

The final result for m_b

$$m_b = 4.86 \pm 0.08\ (\text{exp.})\ \pm 0.39\ (\text{Gen.})\ {}^{+0.02}_{-0.01}\ (\text{ISR})\ {}^{+0.18}_{-0.00}\ (\text{FSR})\ {}^{+0.17}_{-0.00}\ (\text{CR})\ {}^{+0.14}_{-0.13}\ (\Lambda_s)\ \ \text{GeV}$$

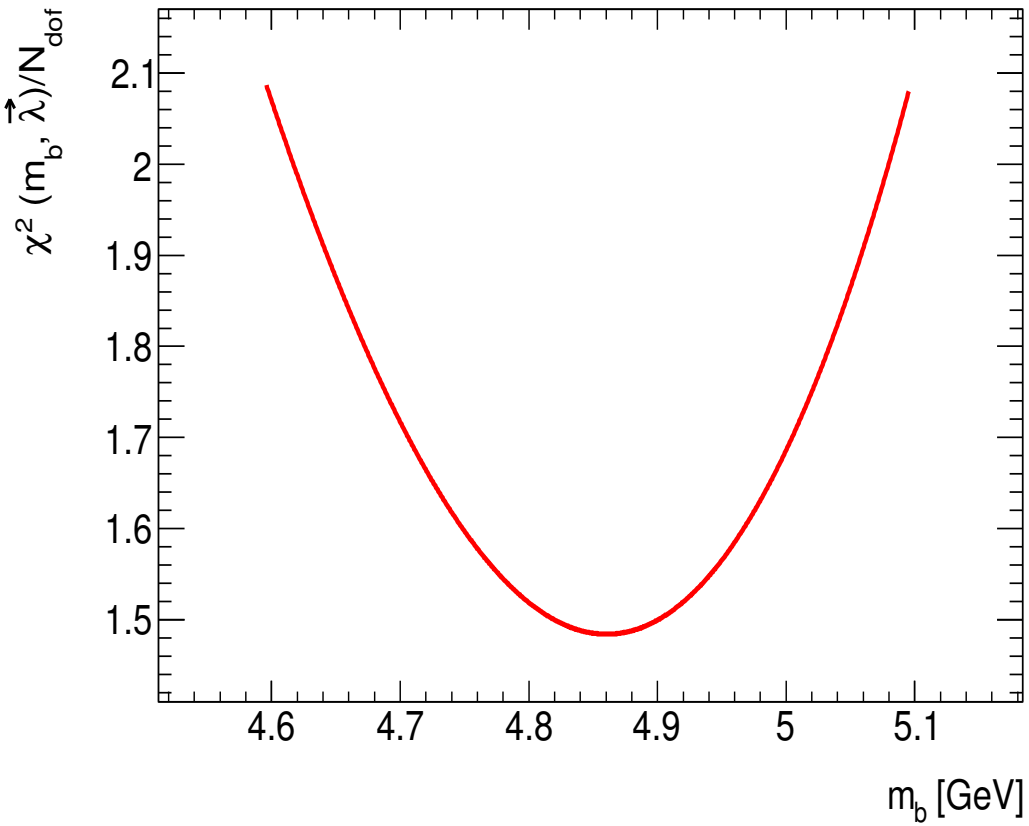

V. TEEC and $\alpha_s(m_Z)$

The ATLAS Collaboration, Phys. Lett. B **750**, 427 (2015)

J. Llorente, F. Barreiro. ATL-COM-PHYS-2013-884

Transverse energy-energy correlations

TEEC: The x_{T}-weighted distribution of differences in azimuth between jets i and j, with $x_{\mathrm{T}i} = \frac{E_{\mathrm{T}i}}{\sum_k E_{\mathrm{T}k}}$

$$\frac{1}{\sigma}\frac{d\Sigma}{d(\cos\phi)} = \frac{1}{\sigma}\sum_{ij}\int \frac{d\sigma}{dx_{\mathrm{T}i}dx_{\mathrm{T}j}d(\cos\phi)} x_{\mathrm{T}i}x_{\mathrm{T}j}dx_{\mathrm{T}i}dx_{\mathrm{T}j}$$

And the azimuthal asymmetry ATEEC is defined as

$$\frac{1}{\sigma}\frac{d\Sigma^{\mathrm{asym}}}{d(\cos\phi)} \equiv \frac{1}{\sigma}\frac{d\Sigma}{d(\cos\phi)}\bigg|_{\phi} - \frac{1}{\sigma}\frac{d\Sigma}{d(\cos\phi)}\bigg|_{\pi-\phi}$$

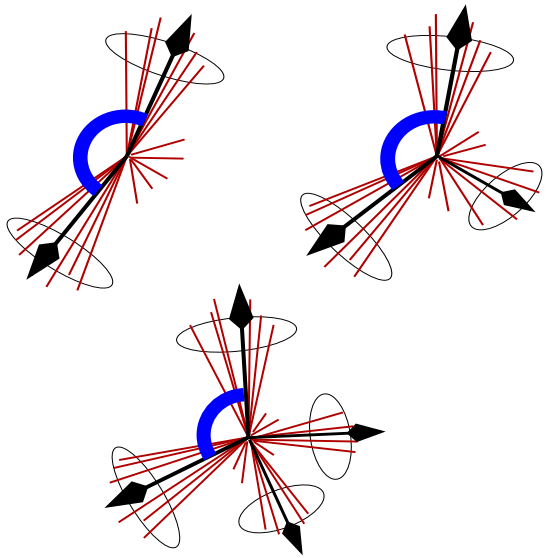

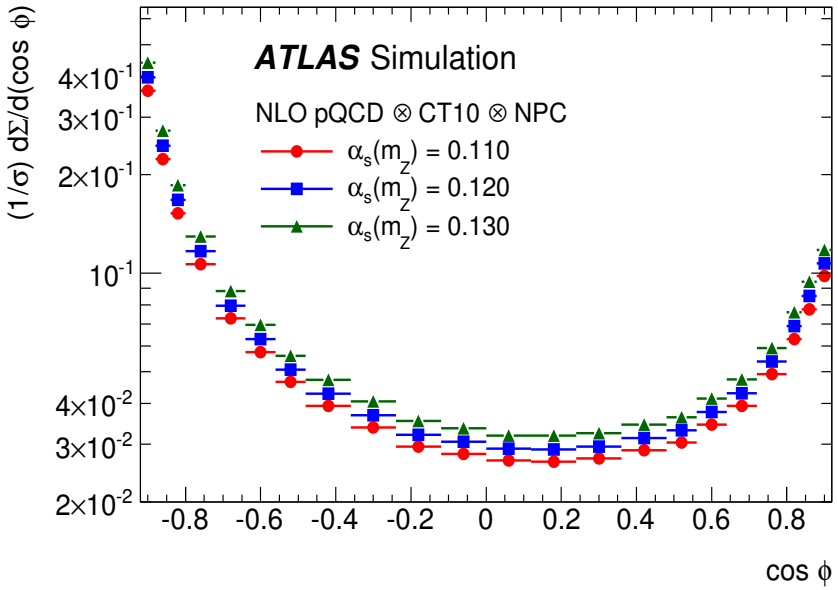

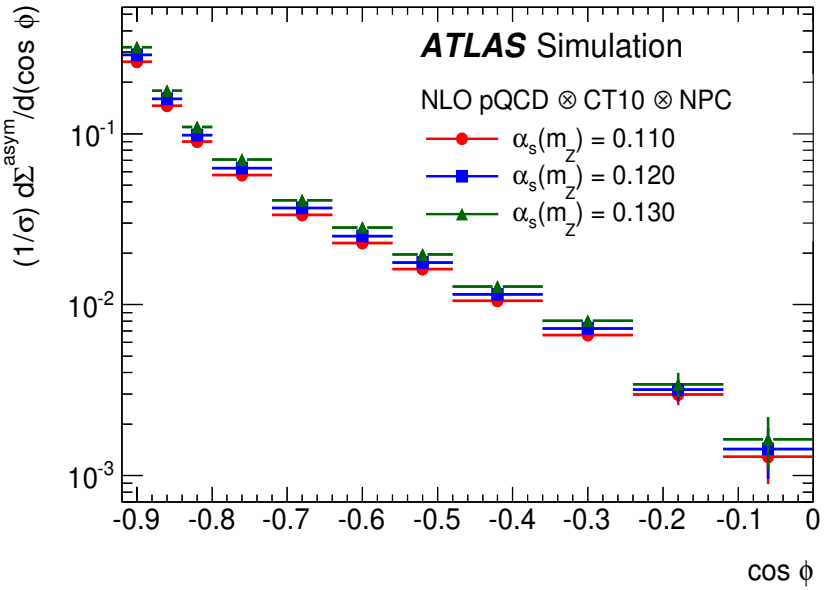

[A. Ali, F. Barreiro, J. Llorente, W. Wang. Phys. Rev. **D86**, 114017 (2012)]

Transverse energy-energy correlations. Properties

The TEEC and ATEEC functions exhibit several advantages:

- Theoretically:
  - Smaller sensitivity to IR divergencies than other event shape variables.
  - NLO corrections are about 10% for ATEEC.
  - Reduced sensitivity to PDFs. μ-uncertainties similar to other cross-section ratios.
- Experimentally:
  - φ^{jet} measured with a very high precision $\Rightarrow$ Migration suppression.
  - The TEEC function is highly stable w.r.t. JES and JER ($w \sim E_i E_j / E^2$).

These measurements extend those of EEC and AEEC which played significant role in determining $\alpha_s(m_Z)$ in e^+e^- colliders.

Event selection

For this measurement, we have selected inclusive multi-jet events in 4.6 fb^{-1} of 2011 data with the following cuts:

- Trigger: EF_j135_a4tc_EFFS.
- Trigger prescale factor of ~ 30 ($\mathcal{L}_{\text{eff}} = 158\ \text{pb}^{-1}$).
- At least one primary vertex with 5 or more tracks with $p_T > 400$ MeV.
- Jet selection: anti-k_T ($R = 0.4$) jets with LC+JES calibration.
- Jet cleaning: Bad and Ugly jets are removed.
- $p_T > 50$ GeV, $|\eta| < 2.5$ and $|\text{JVF}| > 0.75$ for each jet.
- The two leading jets have to fulfill $p_{T1} + p_{T2} > 500$ GeV.

Multijet event displays I (Atlantis)

A dijet event recorded during the 2011 *pp* run is displayed below

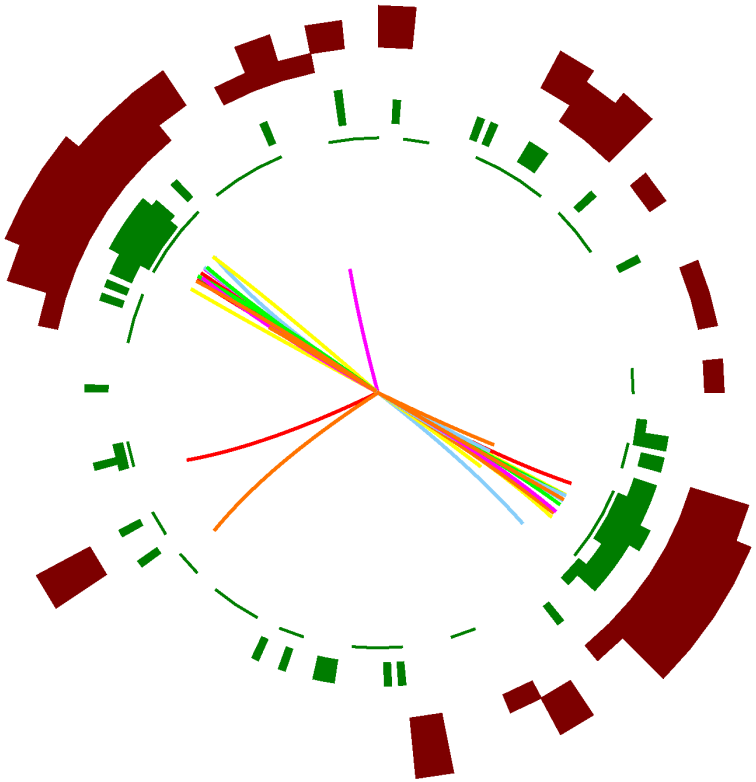

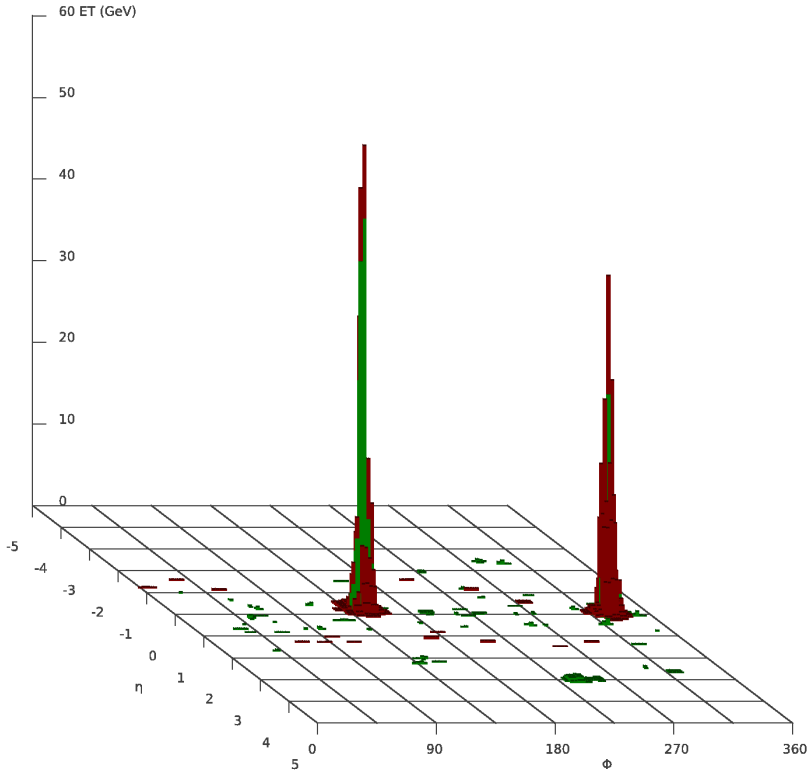

$$\Delta\varphi_{12} \simeq \pi$$

Multijet event displays II (Atlantis)

A three-jet event recorded during the 2011 *pp* run is displayed below

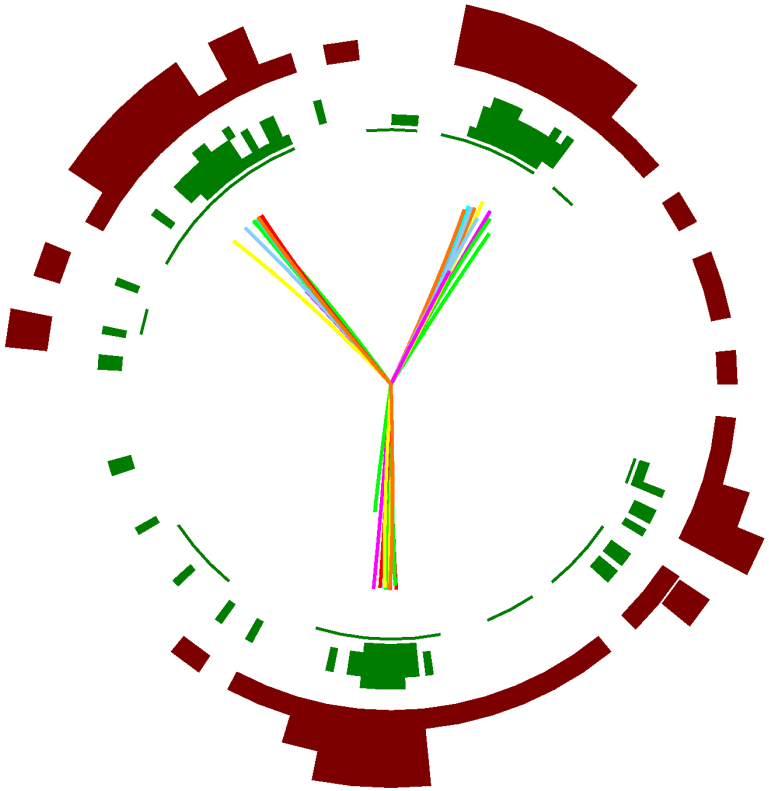

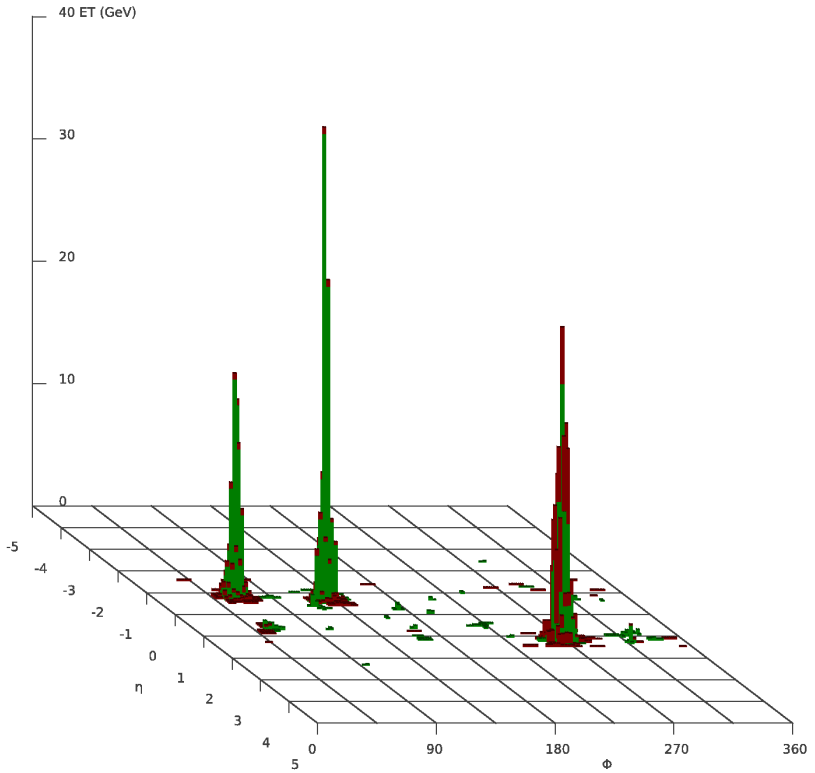

$$\Delta\varphi_{ij} < \pi$$

Control plots

The plots show control distributions for the selected jets, compared to expectations by PYTHIA AUET2B

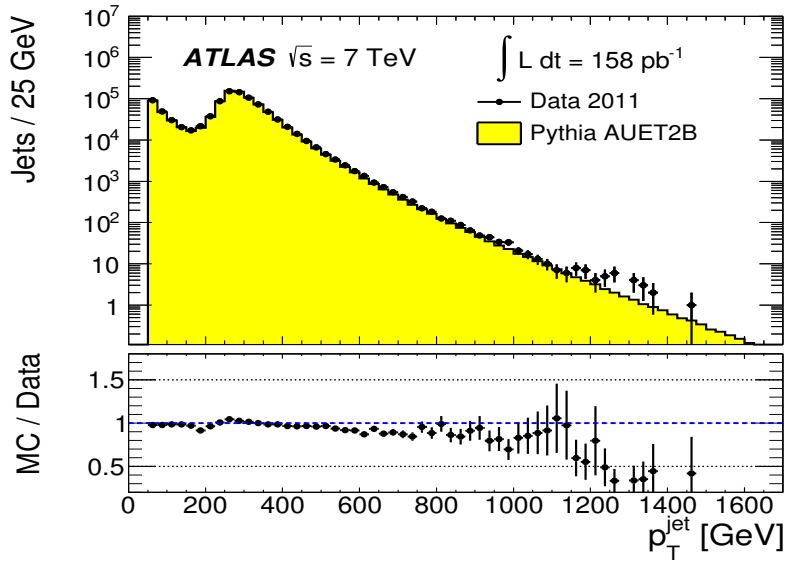

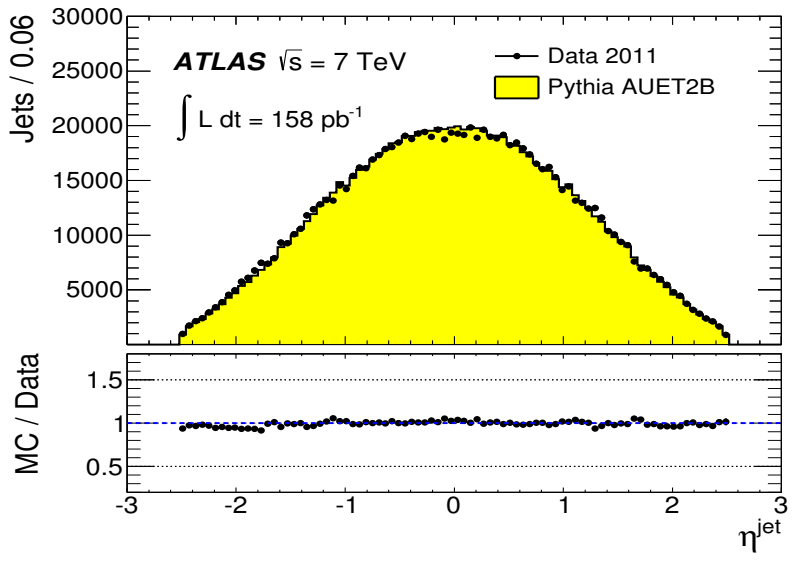

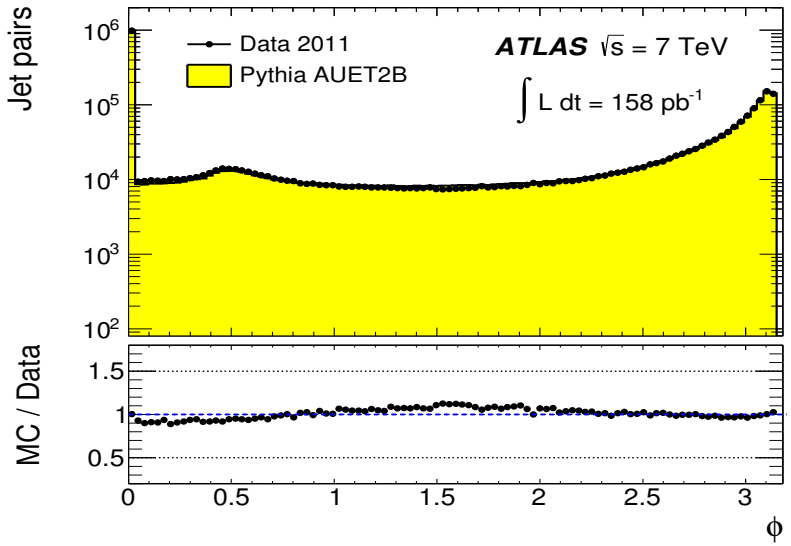

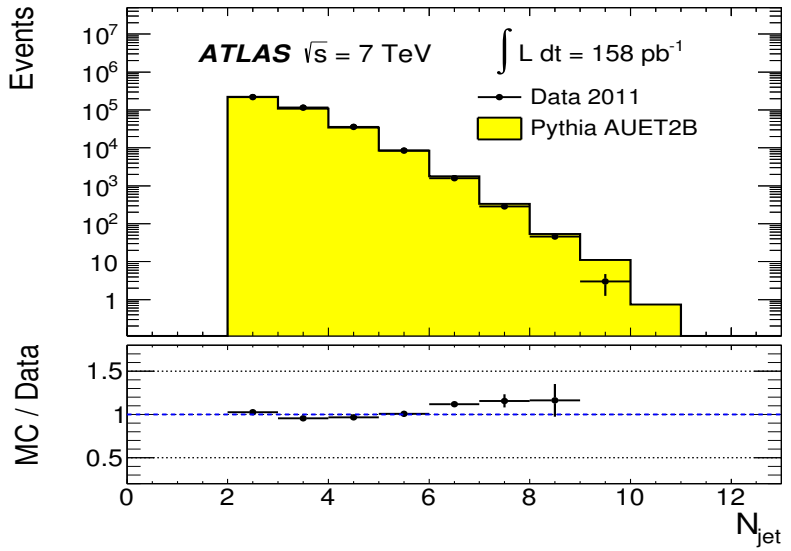

Results at the Detector Level

The plots below show the TEEC and ATEEC functions along with several MC expectations. The error bars in data include statistical uncertainties only.

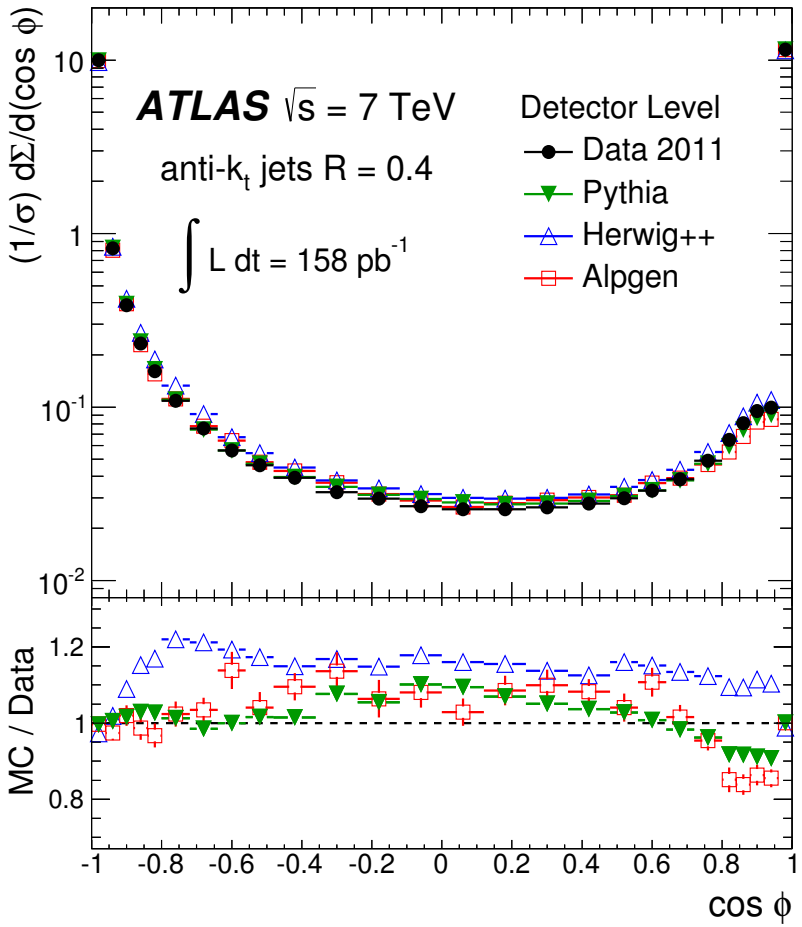

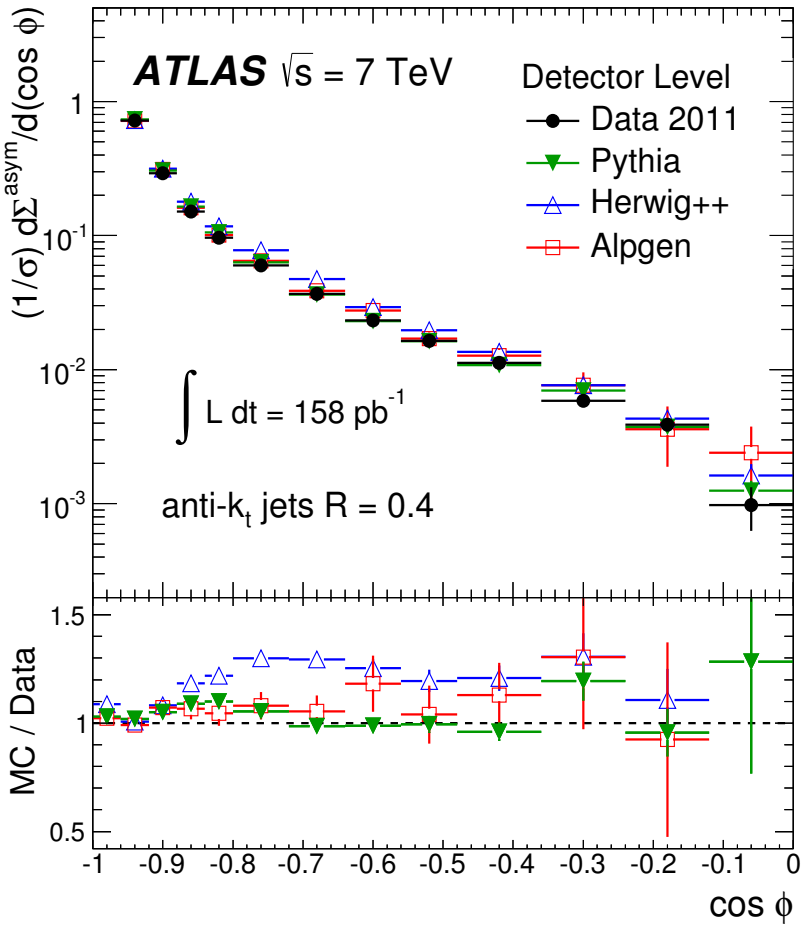

Pythia and Alpgen describe the gross features of the data.

Unfolding

To correct our data for detector effects, we perform a bin by bin unfolding based on the Pythia samples. The unfolding is cross-checked using a matricial approach based on Bayes' theorem.

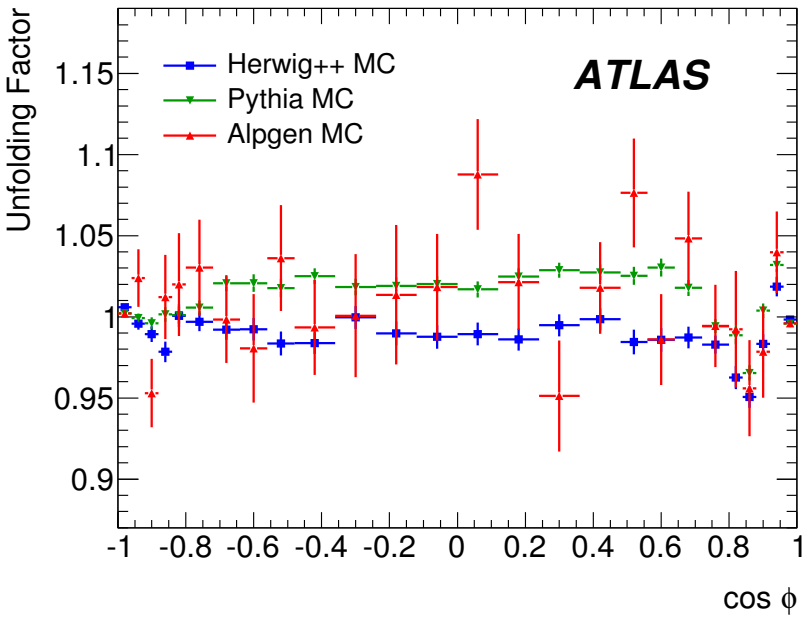

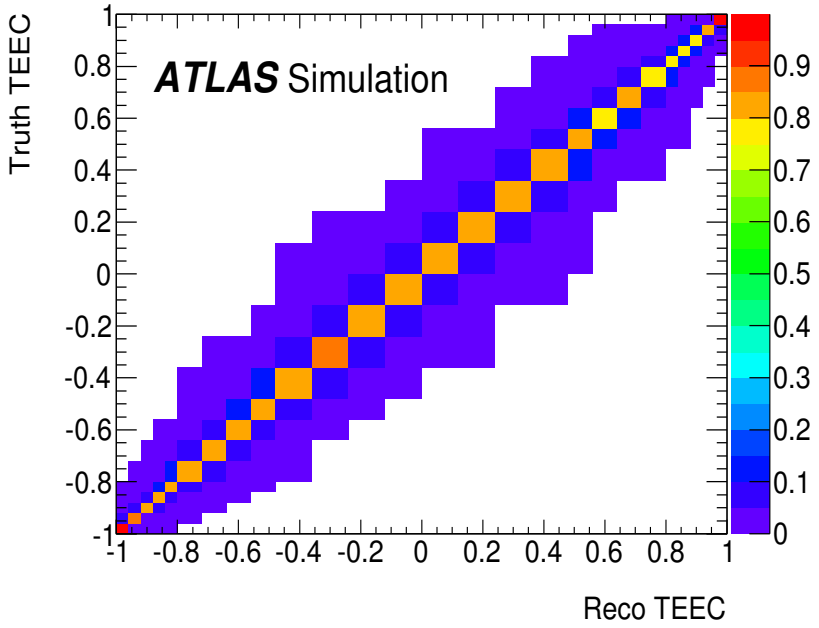

Unfolding: Corrected data

The plots below show the TEEC and ATEEC distributions, corrected for detector effects, compared to the truth level information from various Monte Carlos.

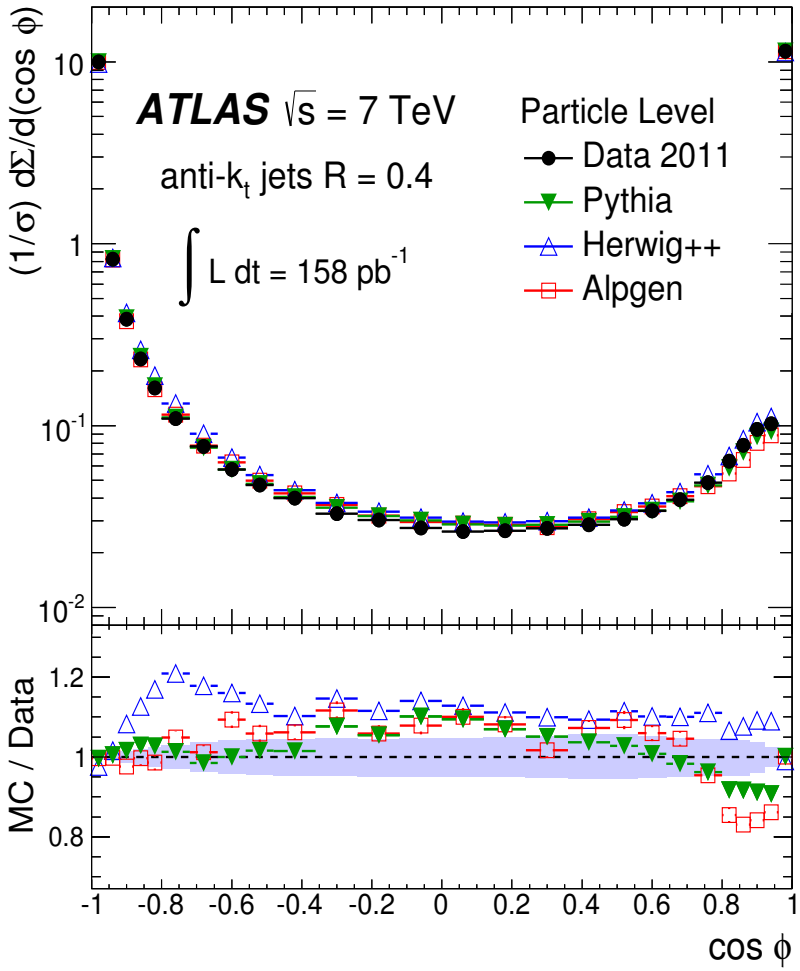

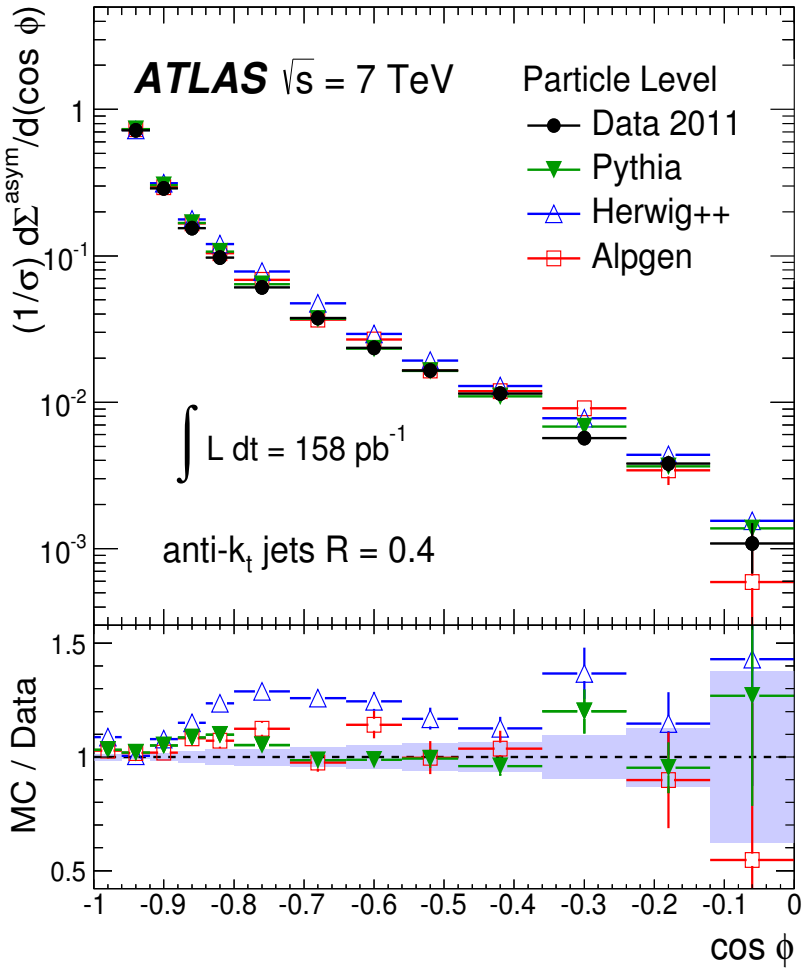

Systematic uncertainties

The main systematic uncertainties are:

- Jet energy scale: Uncertainty on the jet calibration in 61 nuisance parameters. Evaluated by scaling up and down the jet energy and momentum.
- Jet energy resolution: Evaluated by smearing the jet energy and momentum by a smearing factor accounting for finite resolution.
- Shower modelling: The parton shower model in the Monte Carlo used for the unfolding.
- Pileup: How the MC describes the pileup dependence of the observable.
- Unfolding: Effects of the misdescription of the data by the MC model used for unfolding.

Systematic uncertainties

The plots below show the relative systematic uncertainties for the TEEC (left) and ATEEC (right).

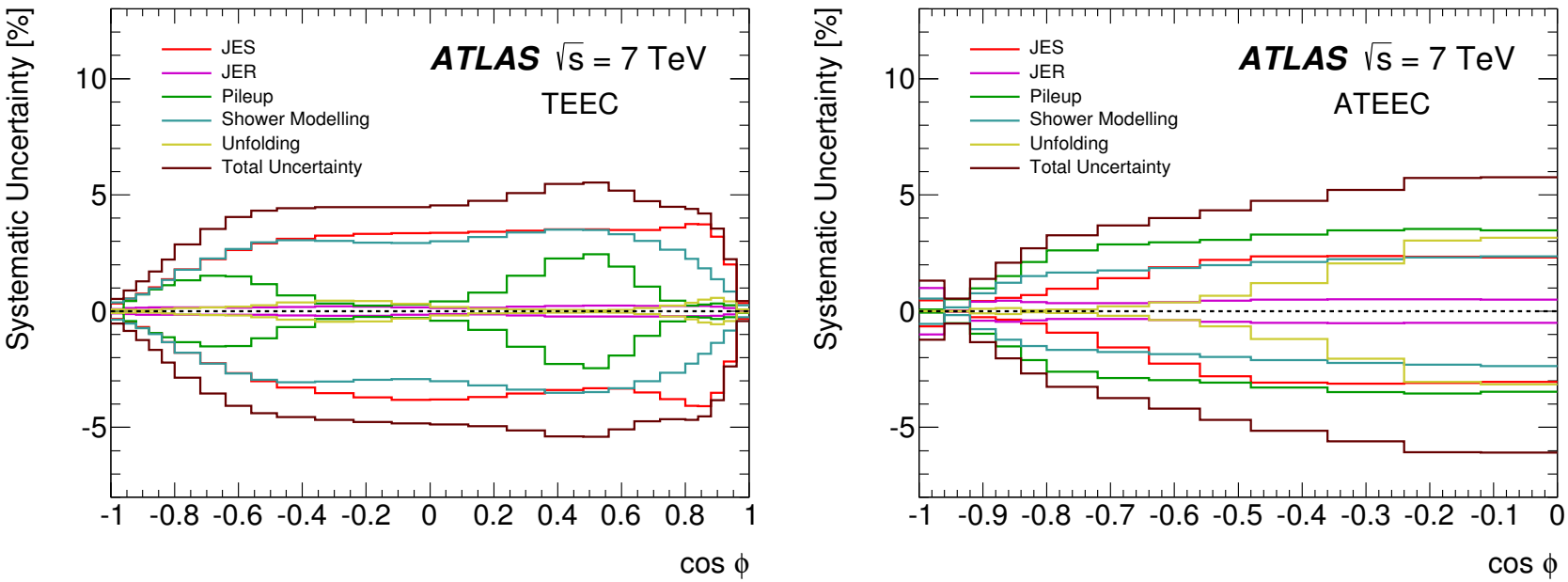

All numbers (including the 61-dimensional breakdown for JES uncertainty) in

http://hepdata.cedar.ac.uk/view/ins1387176

Non-perturbative effects

The plot below shows the total non-perturbative correction

$$\mathcal{F} = \frac{\mathrm{TEEC}(\mathrm{Had} = \mathrm{ON}, \mathrm{UE} = \mathrm{ON})}{\mathrm{TEEC}(\mathrm{Had} = \mathrm{OFF}, \mathrm{UE} = \mathrm{OFF})}$$

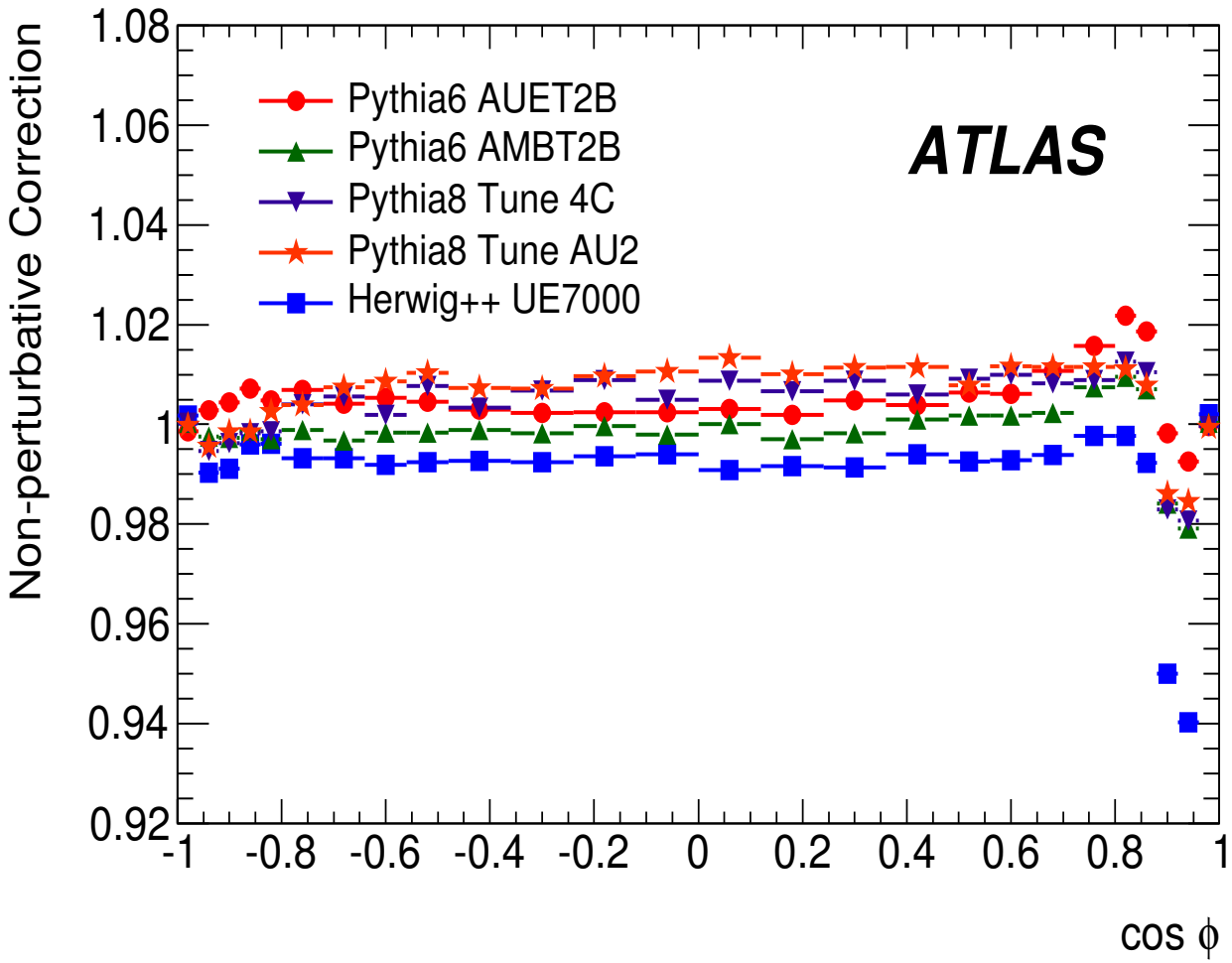

Comparison Data / Theory

- The agreement data / prediction is good within uncertainties.
- Theoretical uncertainties dominated by μ_R, μ_F.

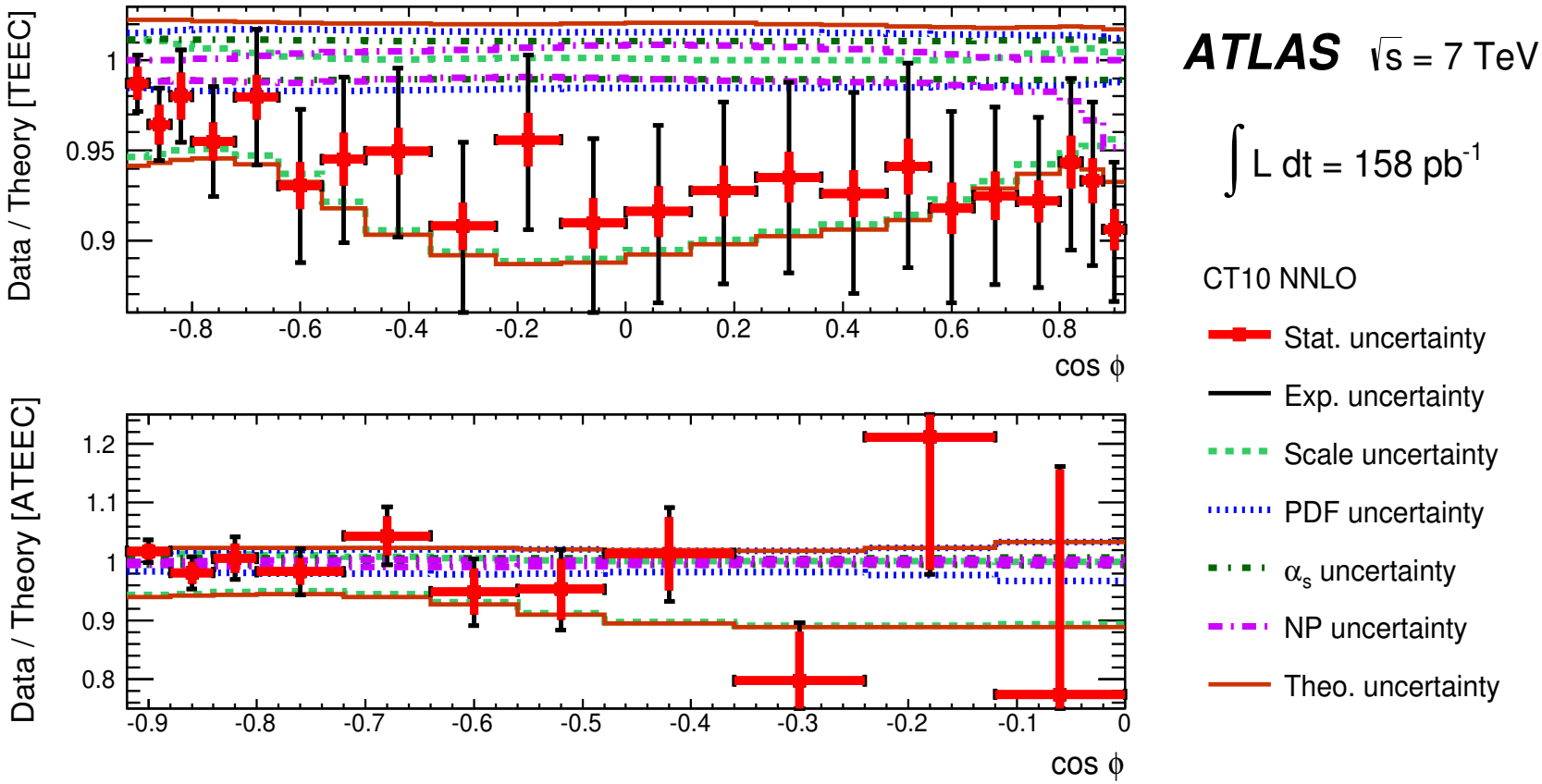

Determination of the strong coupling constant

Again, a standard χ^2 with correlations between uncertainties is used.

$$\chi^2(\alpha_s;\vec{\lambda}) = \sum_k \frac{(x_k - F_k(\alpha_s;\vec{\lambda}))^2}{\Delta x_k^2 + \Delta \tau_k^2} + \sum_i \lambda_i^2$$

$$F_k(\alpha_s;\vec{\lambda}) = \phi_k(\alpha_s)\left(1 + \sum_i \lambda_i \sigma_{ik}\right)$$

The functions $\phi_k(\alpha_s)$ are parameterised using second order polynomials.

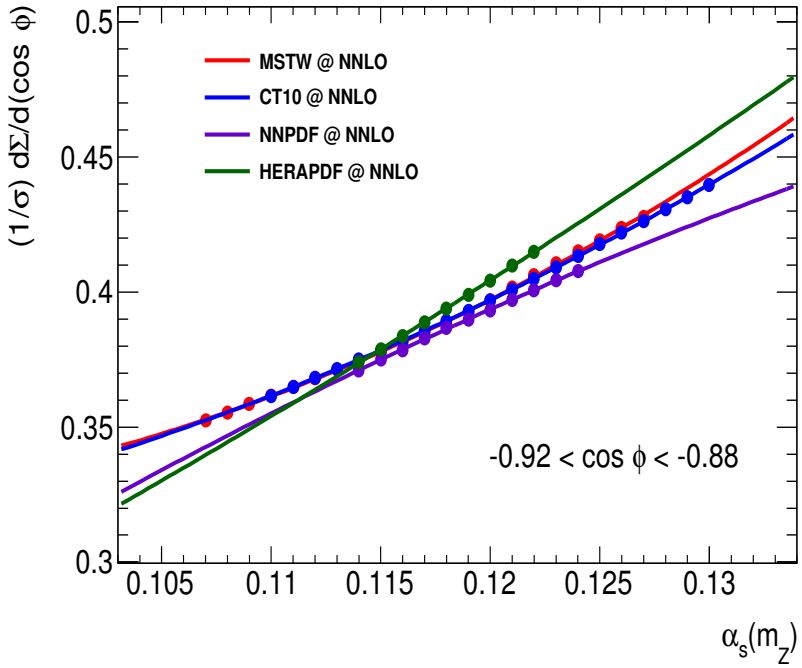

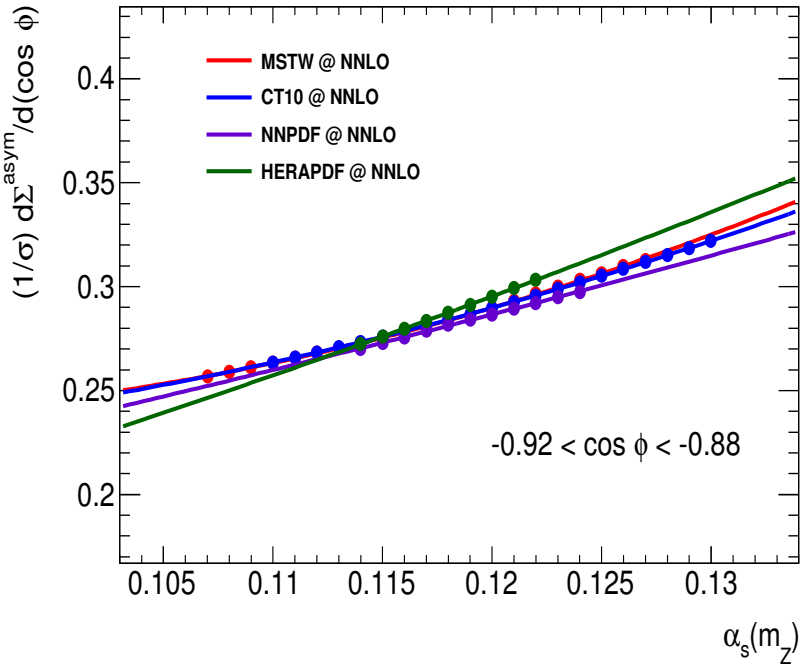

Results for $\alpha_s(m_Z)$

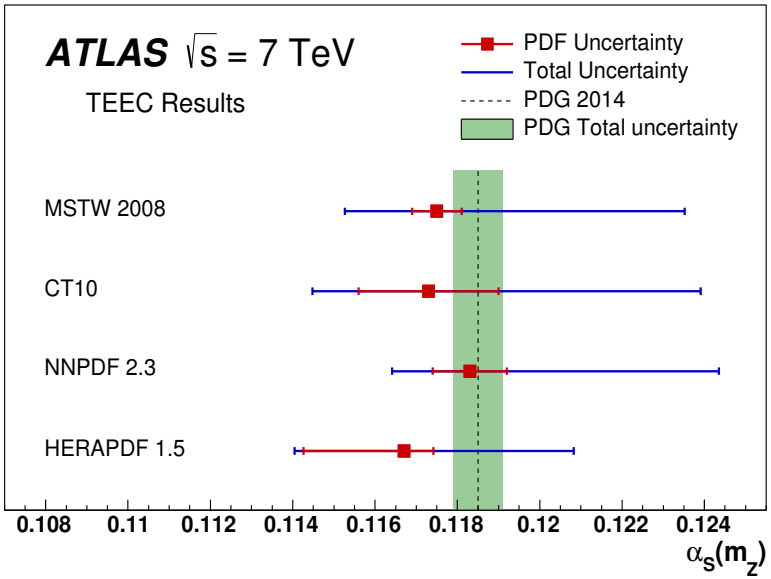

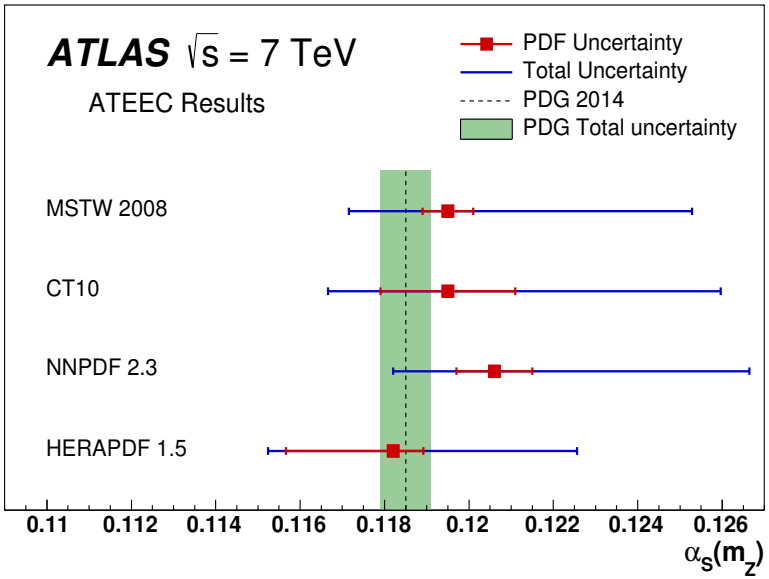

PDF	$\alpha_s(m_Z)$ value (TEEC fit)	χ^2/N_{dof}
MSTW 2008	0.1175 ± 0.0010 (exp.) $^{+0.0059}_{-0.0019}$ (scale) ± 0.0006 (PDF) ± 0.0002 (NPC)	29.0 / 21
CT10	0.1173 ± 0.0010 (exp.) $^{+0.0063}_{-0.0020}$ (scale) ± 0.0017 (PDF) ± 0.0002 (NPC)	28.4 / 21
NNPDF 2.3	0.1183 ± 0.0010 (exp.) $^{+0.0059}_{-0.0013}$ (scale) ± 0.0009 (PDF) ± 0.0002 (NPC)	29.3 / 21
HERAPDF 1.5	0.1167 ± 0.0007 (exp.) $^{+0.0040}_{-0.0008}$ (scale) $^{+0.0007}_{-0.0024}$ (PDF) ± 0.0001 (NPC)	28.7 / 21

PDF	$\alpha_s(m_Z)$ value (ATEEC fit)	χ^2/N_{dof}
MSTW 2008	0.1195 ± 0.0017 (exp.) $^{+0.0055}_{-0.0015}$ (scale) ± 0.0006 (PDF)	12.7 / 10
CT10	0.1195 ± 0.0018 (exp.) $^{+0.0060}_{-0.0015}$ (scale) ± 0.0016 (PDF)	12.6 / 10
NNPDF 2.3	0.1206 ± 0.0018 (exp.) $^{+0.0057}_{-0.0013}$ (scale) ± 0.0009 (PDF)	12.2 / 10
HERAPDF 1.5	0.1182 ± 0.0013 (exp.) $^{+0.0041}_{-0.0008}$ (scale) $^{+0.0007}_{-0.0025}$ (PDF)	12.1 / 10

Fit results

The plots below show the measured TEEC and ATEEC distributions, compared to the results of the fit

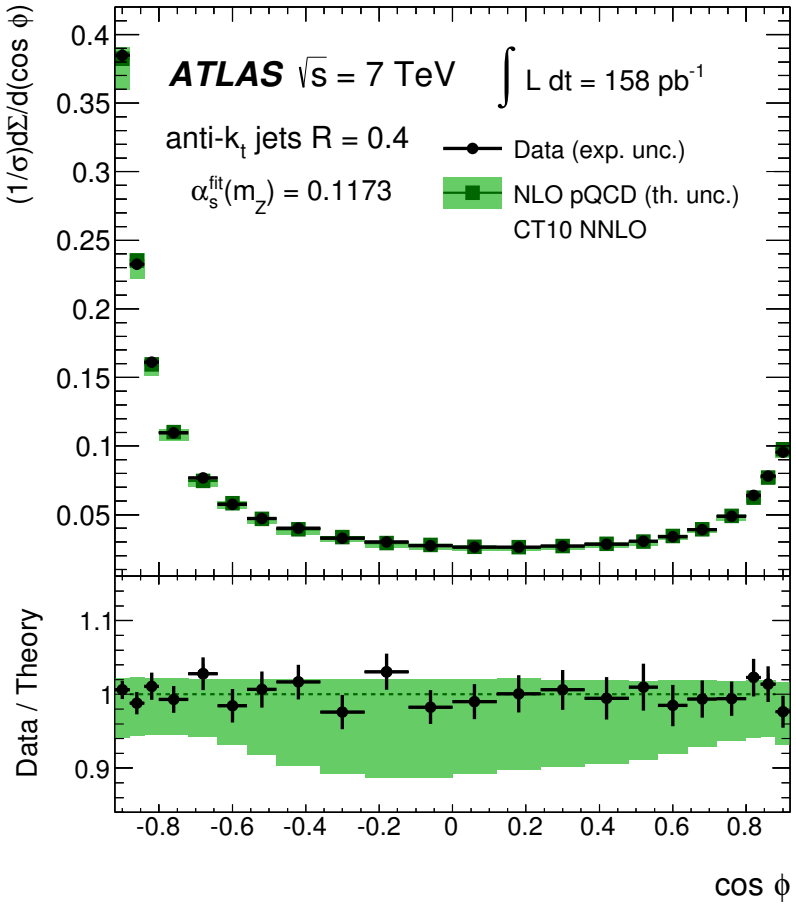

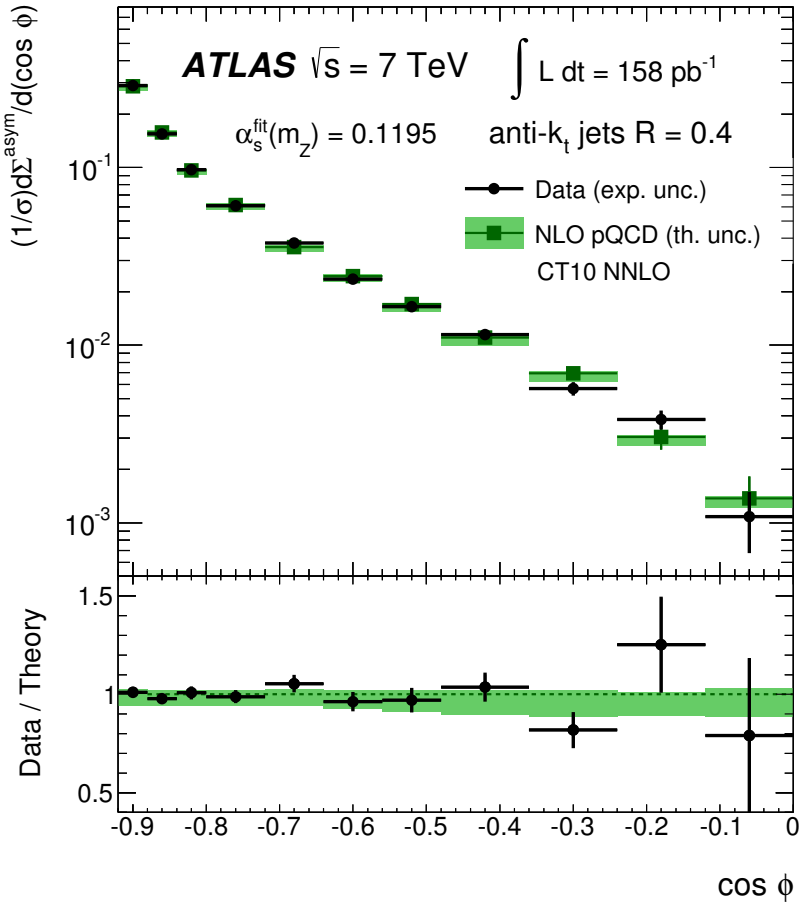

For bin k: $(\Delta x_k)^2 = \sum_{ij} C_{ij}\sigma_i^{(k)}\sigma_j^{(k)}$ with C_{ij} the uncertainty correlation matrix.

Summary of α_s determinations

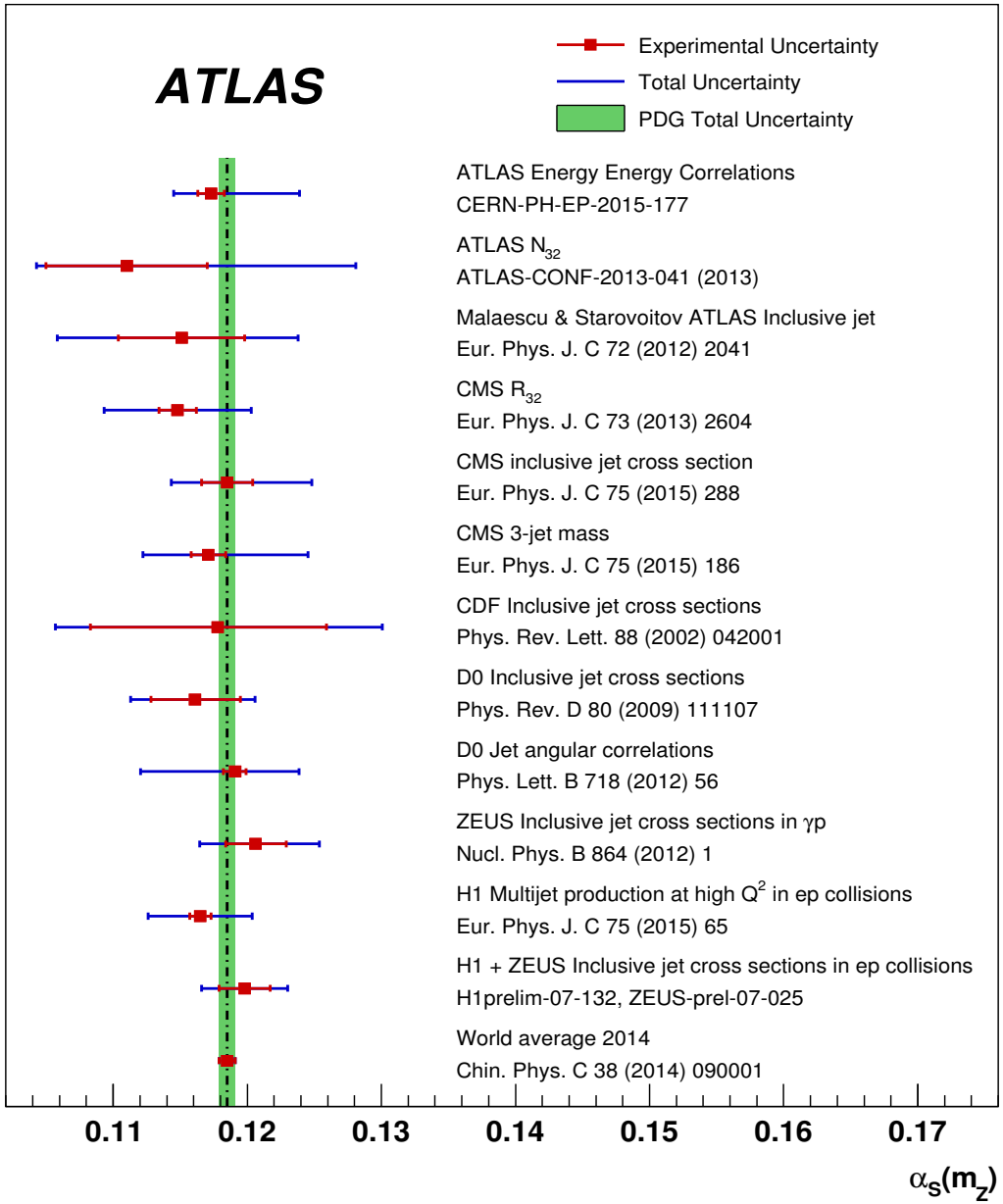

Summary of α_s determinations

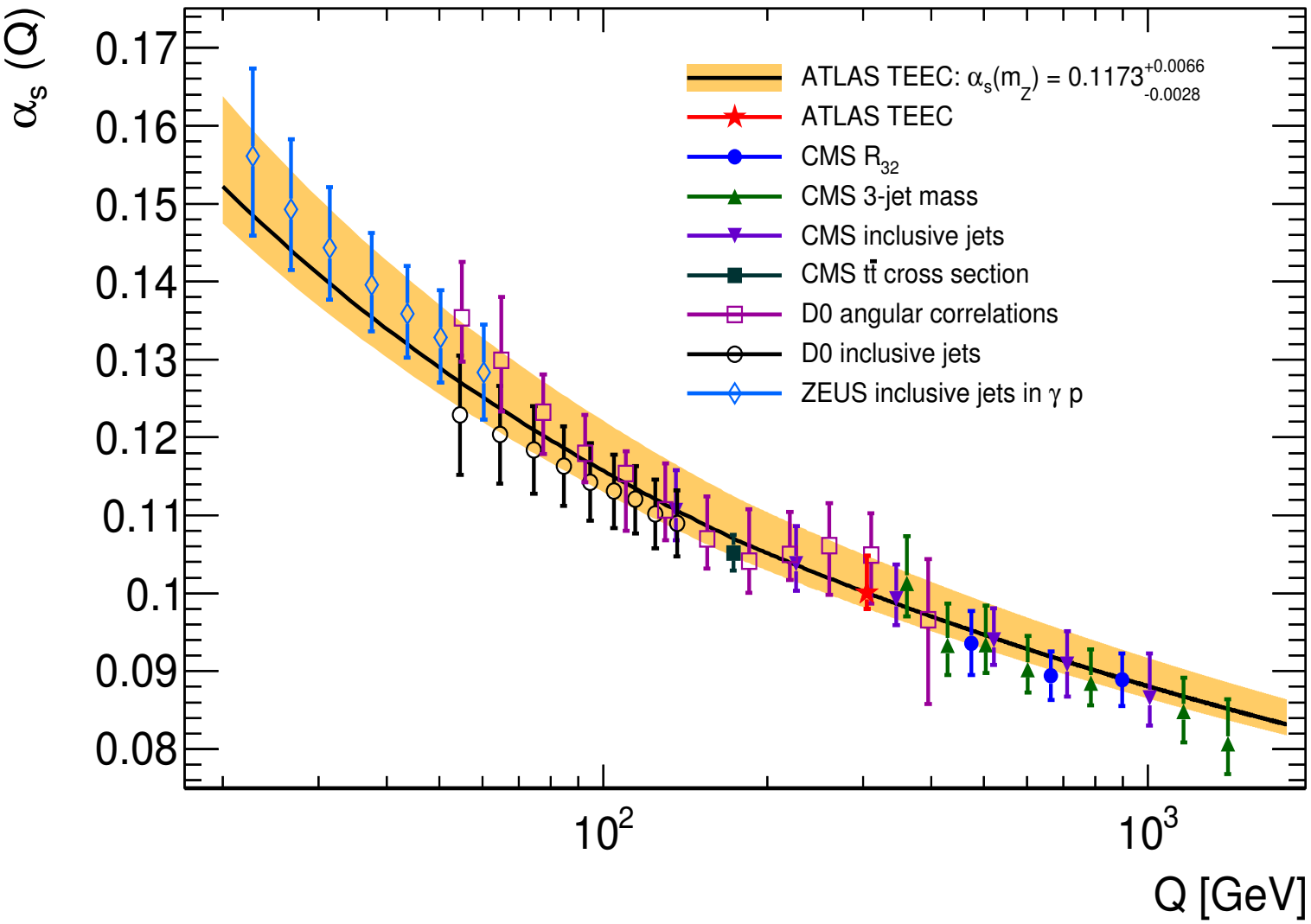

Conclusions (I)

- The analysis of jet shapes brings new insight into the jet structure of $t\bar{t}$ final states for b (light) jets coming from top (resp. W) decays.
- They are strongly (mildly) dependent on the jet p_T (resp. η)
- b-jets are wider than light jets, due to the heavier mass of the b-quark.
- Both light- and b-jets are fairly well described by MC with matrix elements up to NLO matched to parton showers.
- First extraction of the mass of the b-quark using jet substructure.
- Light-jet shapes do not depend on m_b, but do depend on Λ_s.
- The jet shapes of b-quark jets depend on both Λ_s and m_b and can be used for the extraction of the bottom mass, leading to $m_b = 4.86^{+0.49}_{-0.42}$ GeV.
- First measurement of the jet-based transverse energy-energy correlations and its asymmetry at a hadron collider.
- The TEEC and ATEEC at large angles ($|\cos\phi| < 0.92$) provide a stringent test of fixed order pQCD.

Conclusions (II)

- For $\cos\phi \sim \pm 1$, TEEC measurement is sensitive to higher order corrections.
- The TEEC and ATEEC are very sensitive to the value of α_s and show reduced sensitivity to the PDFs.
- The fits to the TEEC and ATEEC distributions determine values of $\alpha_s(m_Z)$ which are compatible between them and with the current world average.
- The extracted value is $\alpha_s(m_Z) = 0.1173 \pm 0.0010\ (\text{exp.})\ ^{+0.0065}_{-0.0026}\ (\text{theo.})$
- The TEEC measurement is limited by the theoretical scale uncertainties.

All the stuff (and more) in:

[The ATLAS Collaboration, Eur. Phys. J. **C73** 2676 (2013)]
[J. Llorente and J. Cantero, Nucl. Phys. B **B889** 401-418 (2014)]
[The ATLAS Collaboration, Phys. Lett. B **750**, 427 (2015)]
Rivet routines are available in https://rivet.hepforge.org/analyses

Backup Slides

Unfolded results: 70 GeV $< p_T <$ 100 GeV

Differential $\langle \rho(r) \rangle$

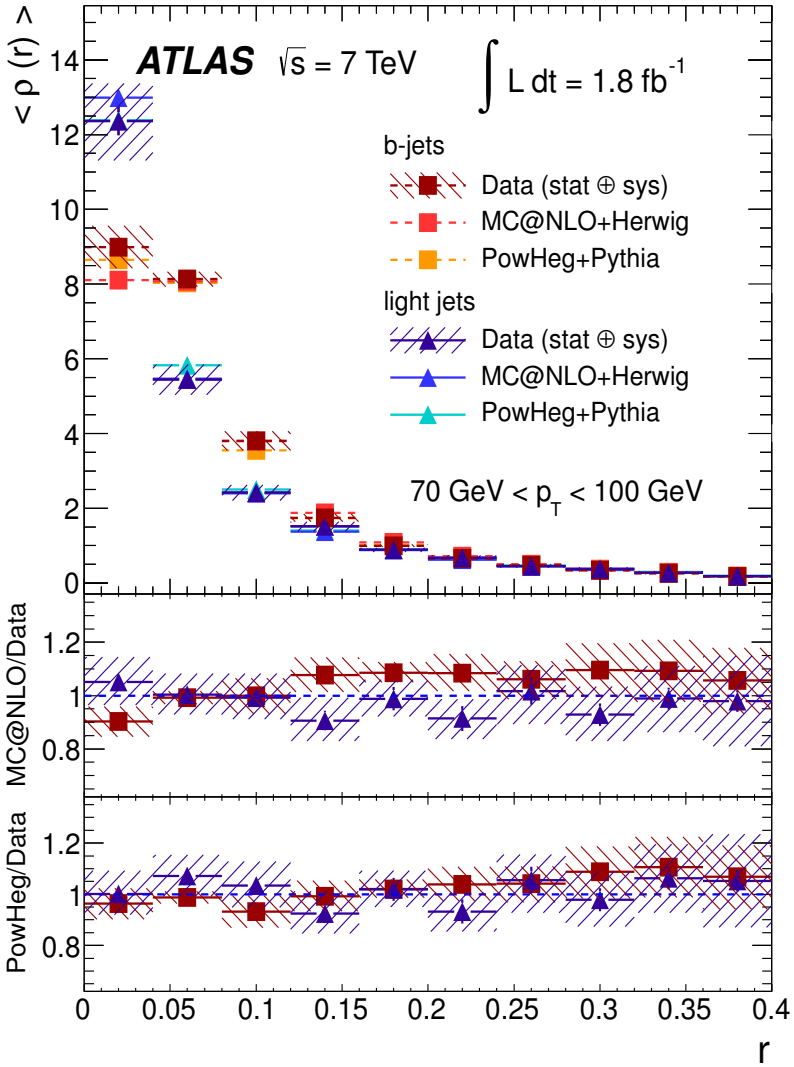

Integrated $\langle \Psi(r) \rangle$

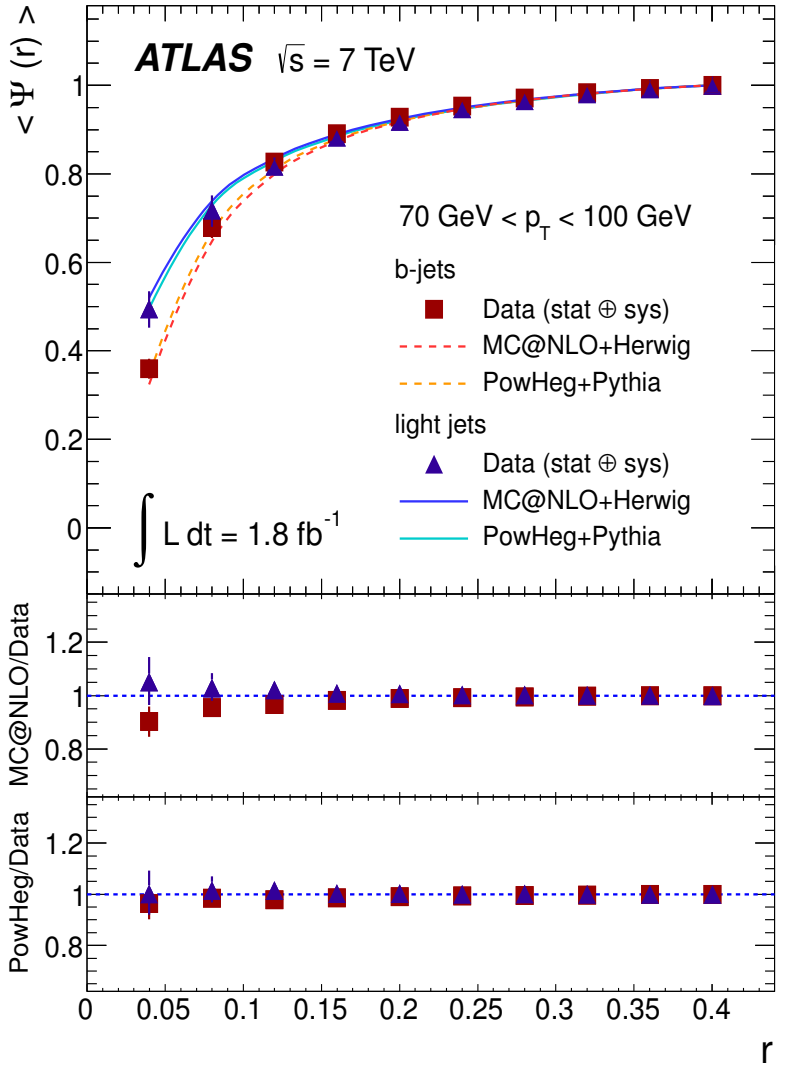

Unfolded results: 100 GeV $< p_T <$ 150 GeV

Differential $\langle \rho(r) \rangle$

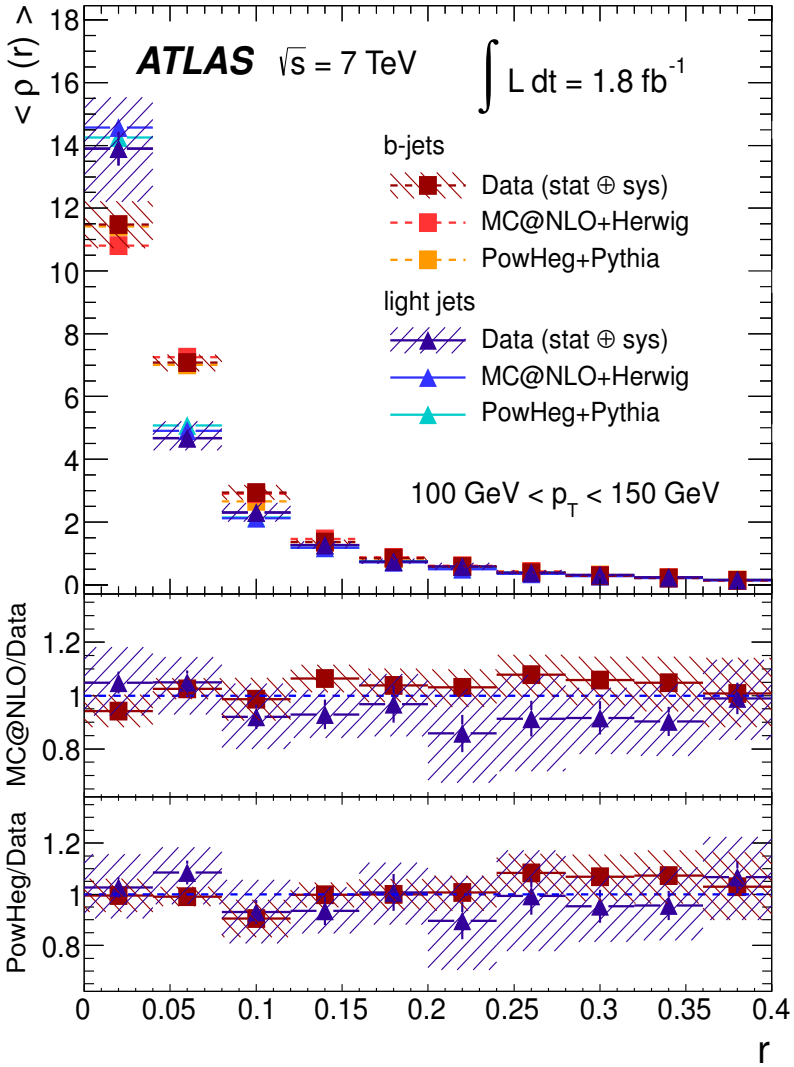

Integrated $\langle \Psi(r) \rangle$

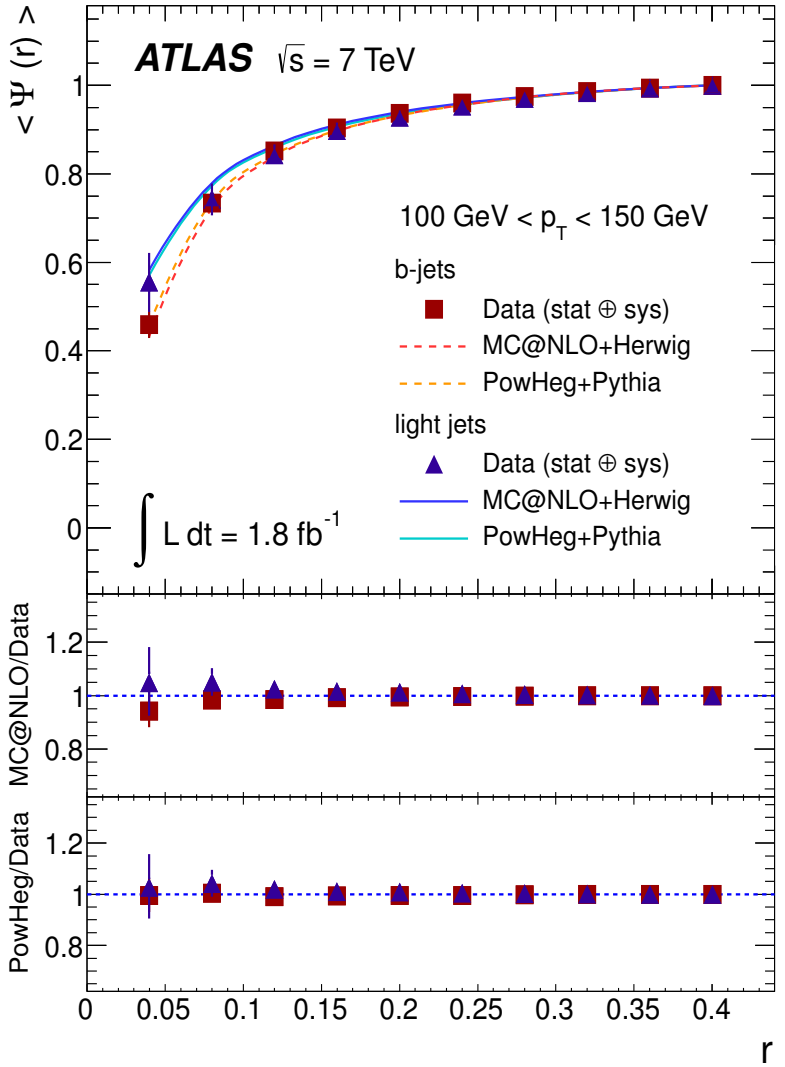

The JVF algorithm

- Variable defined for each jet and vertex (i, j).
- Fraction of p_T of tracks in the jet i associated with the vertex j
- When defined with respect to the primary interaction vertex, it provides rejection power against pileup jets. ($|JVF| > 0.75$)

$$\mathrm{JVF}(\mathrm{jet_i}, \mathrm{vtx_j}) = \frac{\sum_k p_T(\mathrm{trk_k^{jet_i}}, \mathrm{vtx_j})}{\sum_n \sum_l p_T(\mathrm{trk_l^{jet_i}}, \mathrm{vtx_n})}$$

Background estimation

Multi-jet background estimation using jet-electron method
[Phys. Lett. B **717**, 330 (2012)]

- Fake lepton selection from high EM-fraction jets (jet-electron).
- Shape of the distributions estimated accordingly.
- Normalisation derived using binned-likelihood fit to the E_T^{miss} distribution.
- Same method used for muons.

All other backgrounds (W/Z+jets, Single top, ...) estimated using MC simulation.

ΔR distributions

The distributions of ΔR_{jj} for b (left) and light jets (right).

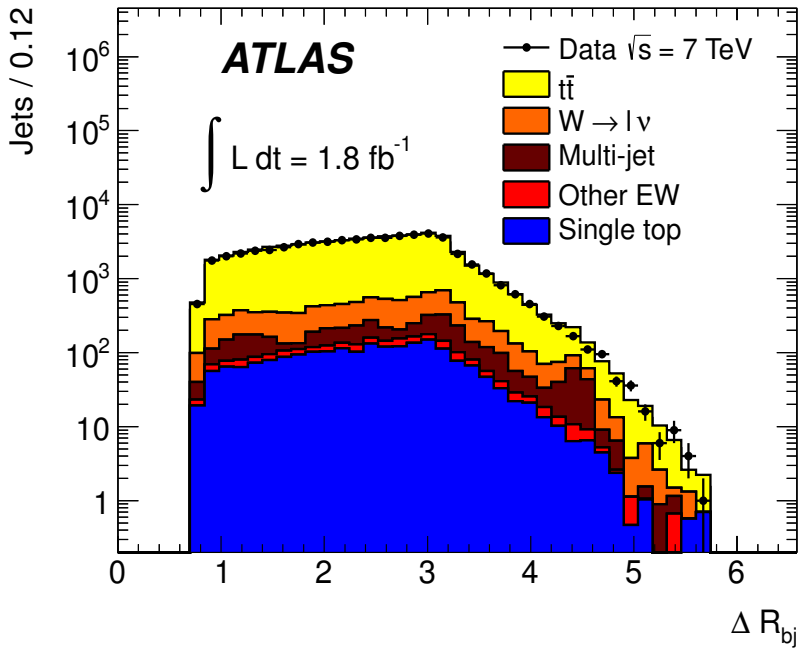

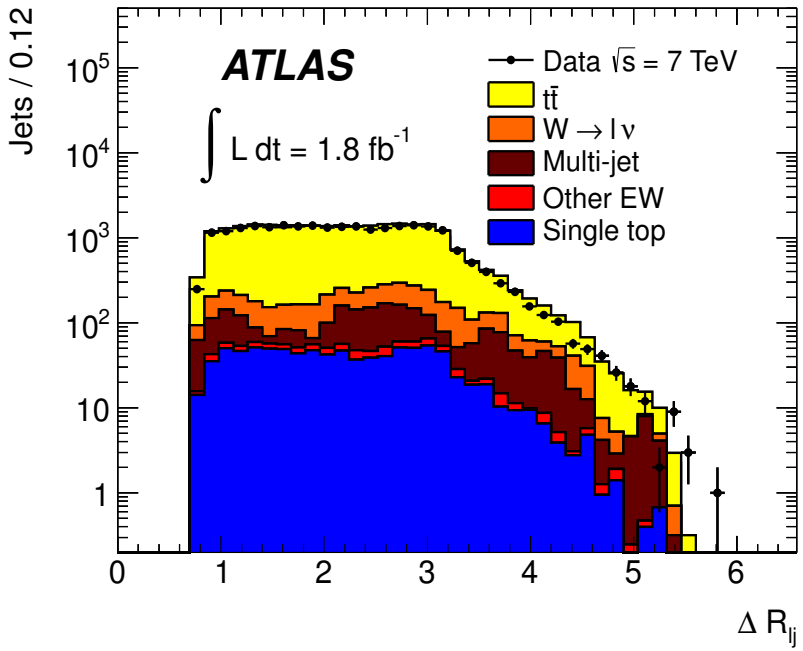

Theoretical uncertainties on m_b (I): Generator modelling

The extraction of m_b has been repeated using HERWIG++. This accounts for differences in the parton shower modelling and non-perturbative effects.

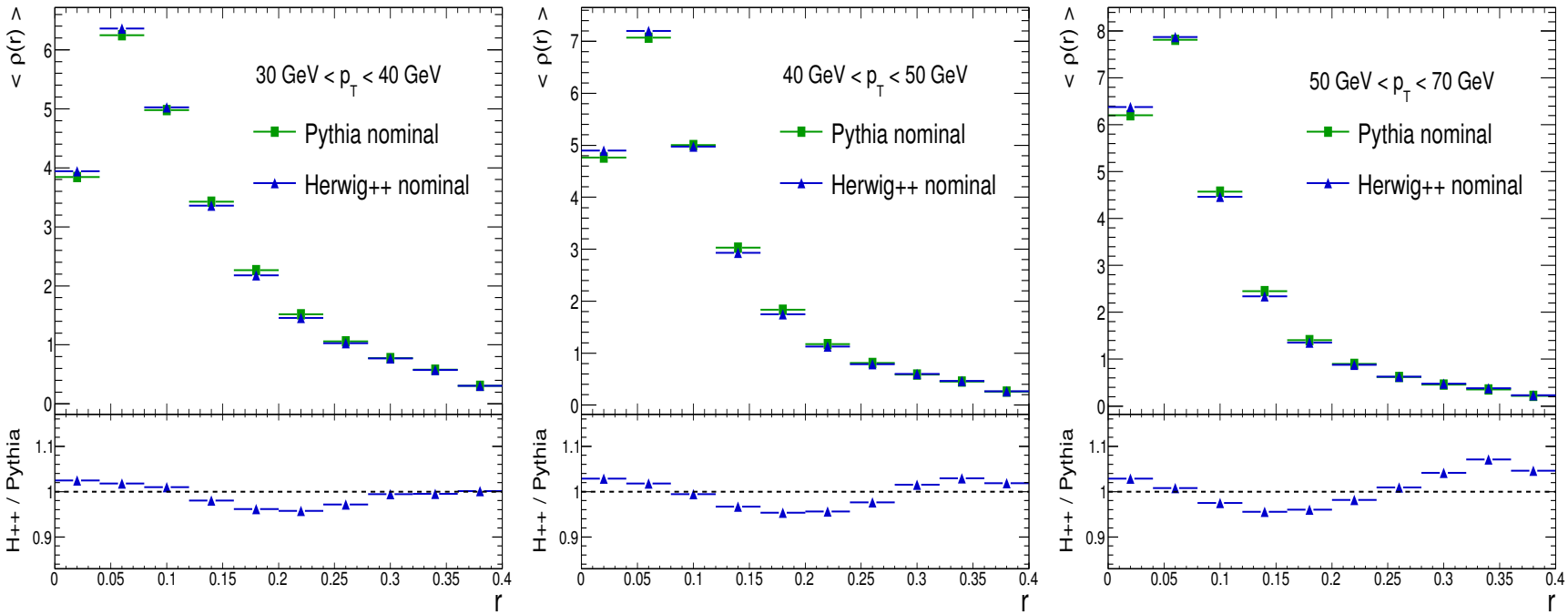

The value of Λ_s is set to 160.7 MeV, and leads to $m_b = 5.25 \pm 0.09$ GeV.
The impact on the bottom quark mass is then almost 400 MeV.

Theoretical uncertainties on m_b (II): Initial-state radiation

The PYTHIA parameters controlling ISR, $\mathrm{PARP}(67)$ and $\mathrm{PARP}(64)$, are varied according to the studies made for other ATLAS papers

[The ATLAS Collaboration, Eur. Phys. J. **C72**, 2043 (2012)]

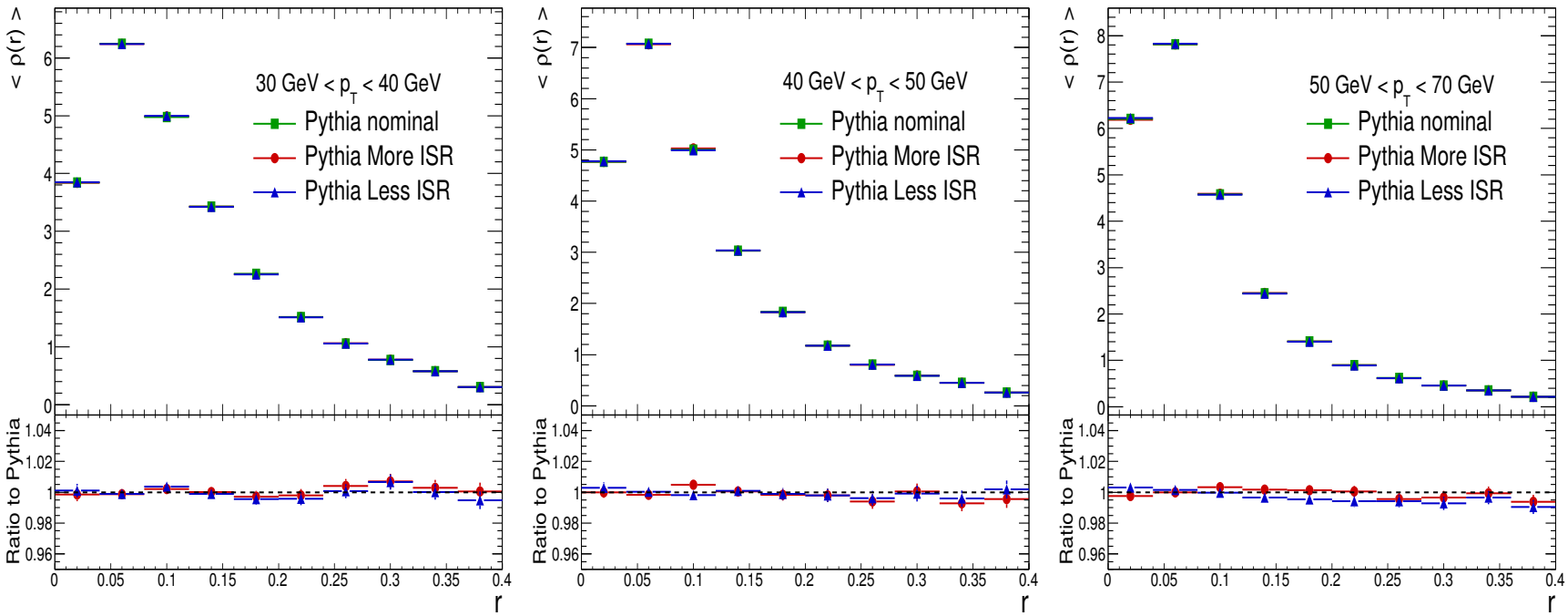

The impact on the bottom mass is around 20 MeV (Relative variation of 0.4%)

Theoretical uncertainties on m_b (III): Final-state radiation

The PYTHIA parameters controlling FSR, $\mathrm{PARP}(72)$ and $\mathrm{PARJ}(82)$, are varied up and down on a factor of 2.

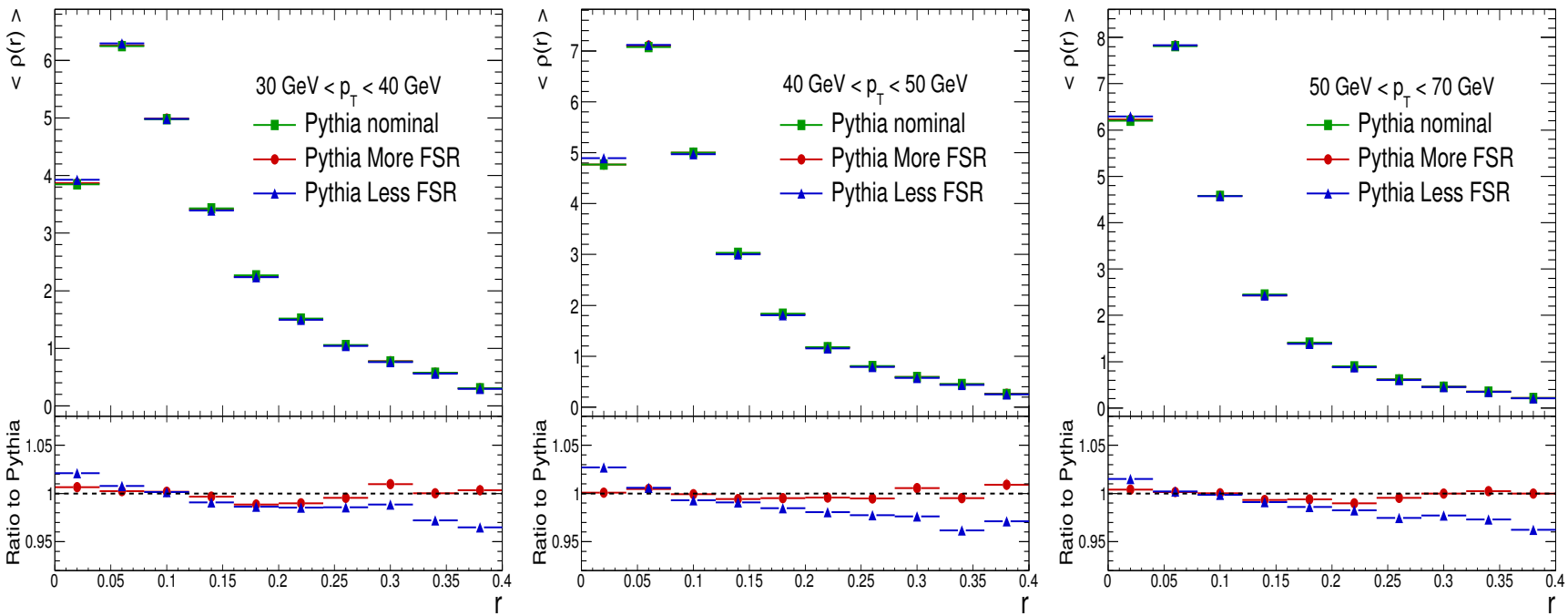

The impact on the bottom mass is around 180 MeV (Relative variation of 4%)

Theoretical uncertainties on m_b (IV): Colour reconnection

The effects of colour reconnection are investigated by using PYTHIA 6.4 + TUNE A CR

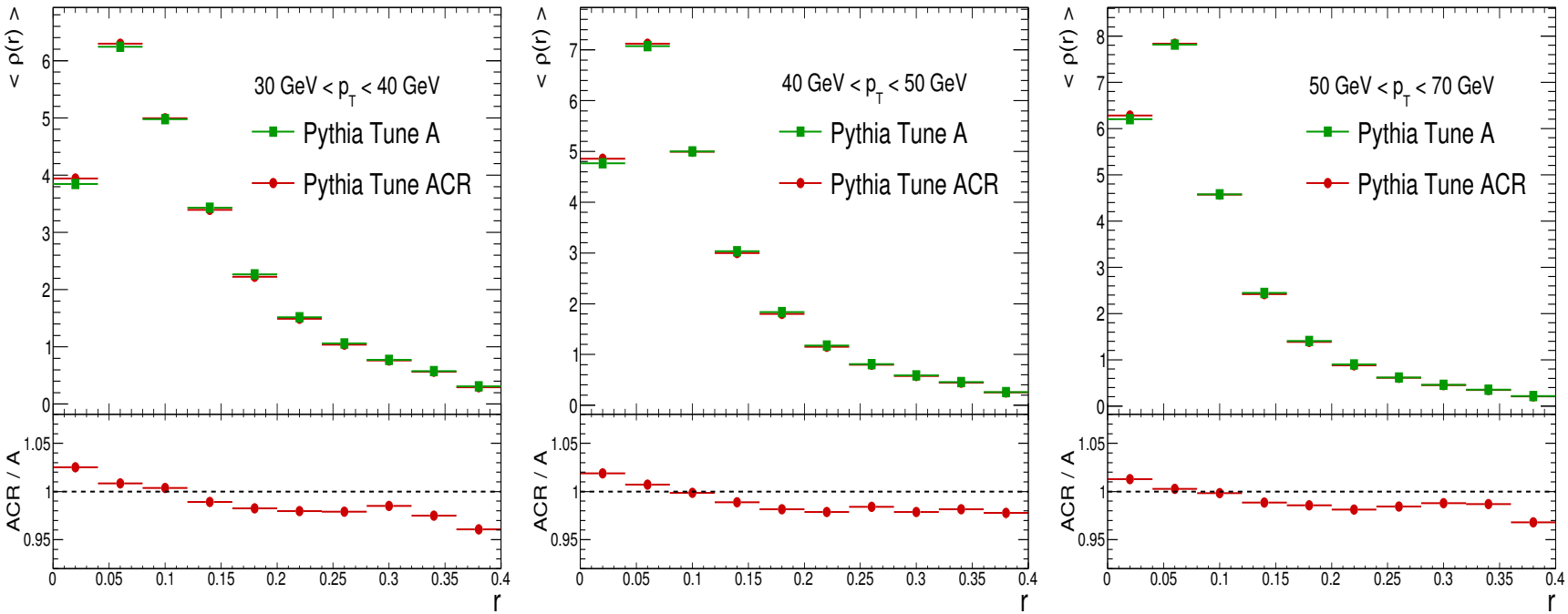

The impact on the bottom mass is 170 MeV (Relative variation of 3.5%)

Theoretical uncertainties on m_b (V): Choice of the Λ_s scale and order of the RGE.

The parton shower scale is varied up and down according to its uncertainty

- Full m_b variations are obtained for $\Lambda_s = 152.5$ MeV and $\Lambda_s = 171.7$ MeV.
- Fits are recalculated to keep track of the (Λ_s, m_b) correlations.
- The impact on the bottom mass is around 60 MeV (about 1.2%).

An additional uncertainty accounts for differences in the determination of m_b using the NLO vs LO expression for the running coupling $\alpha_s(Q^2)$ in the HERWIG++ shower

- Using the NLO solution $\Lambda_s = 276.1 \pm 17.3$ MeV $\Rightarrow m_b = 5.39 \pm 0.08$ GeV
- This is to be compared with $m_b = 5.25 \pm 0.09$ GeV $\Rightarrow \Delta m_b/m_b \simeq 2.7\%$

These two uncertainties are added in quadrature, giving a maximum variation of 140 MeV.

Fit results for Λ_s: Nuisance parameters.

The plots below show the values for the nuisance parameters $\{\lambda_i\}$ and the correlation matrix between them (and Λ_s) for the global fit to the parton shower scale Λ_s.

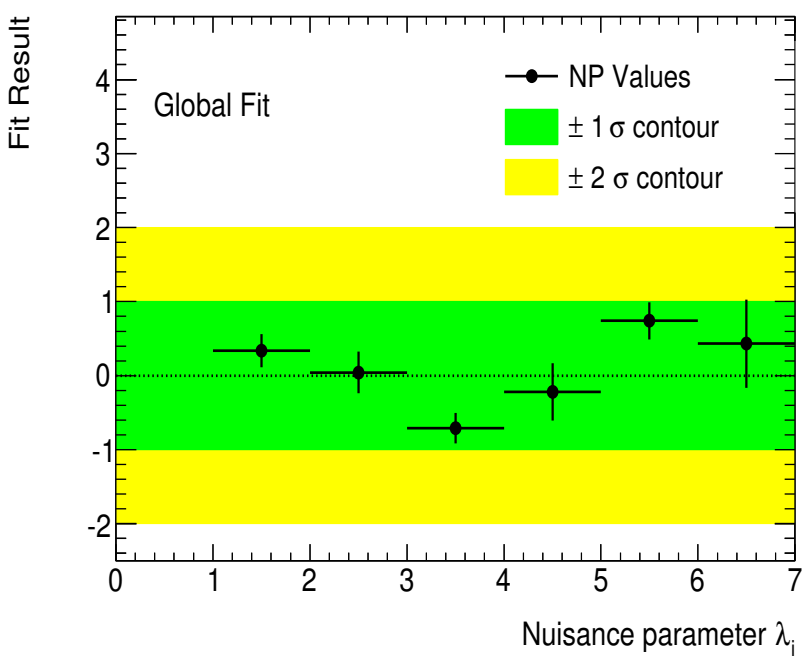

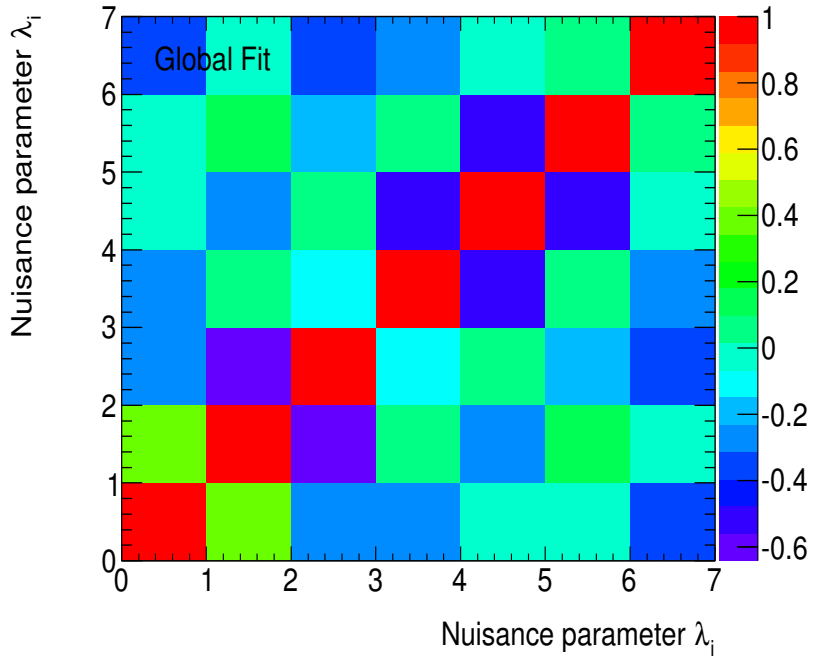

- The values of the nuisance parameters are contained in the $\pm 1\sigma$ region.
- Some (anti-) correlations are seen for the off-diagonal coefficients.

Fit results for m_b: Nuisance parameters.

The plots below show the values for the nuisance parameters $\{\lambda_i\}$ and the correlation matrix between them (and m_b) for the global fit to the b-quark mass m_b.

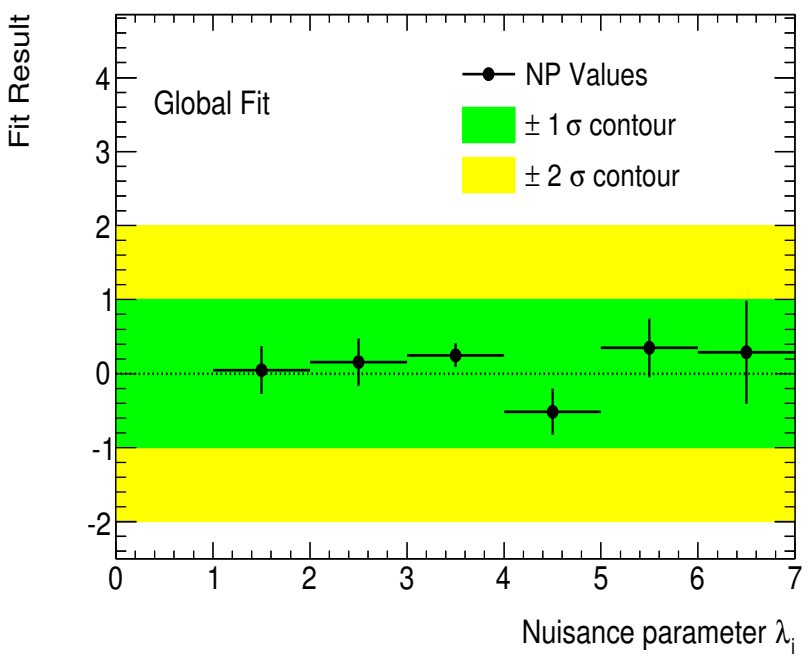

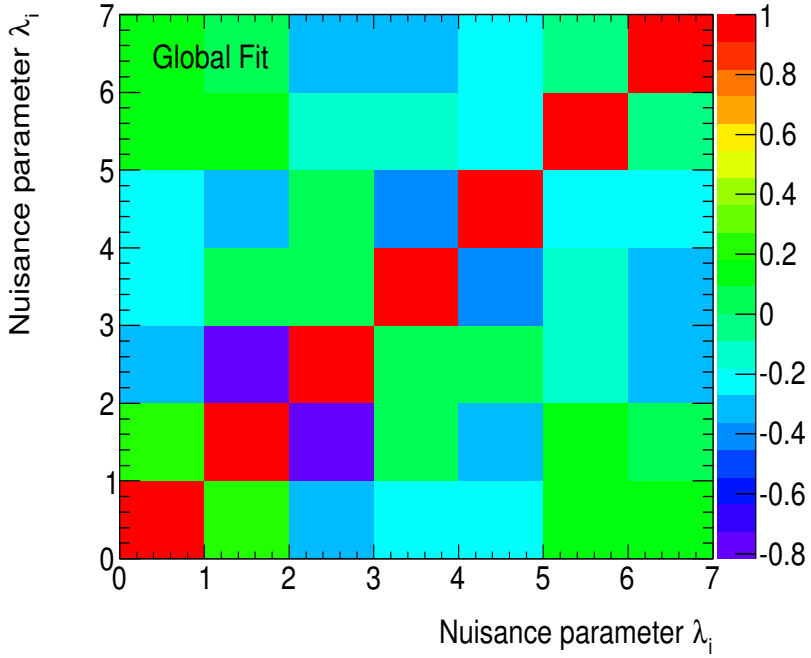

- The values of the nuisance parameters are contained in the $\pm 1\sigma$ region.
- Some (anti-) correlations are seen for the off-diagonal coefficients.

TEEC unfolding: Statistical uncertainty

The statistical uncertainty is derived using the bootstrap method. The bootstrap samples for the unfolding factor are shown on the left, while the composition of the statistical error is shown on the right.

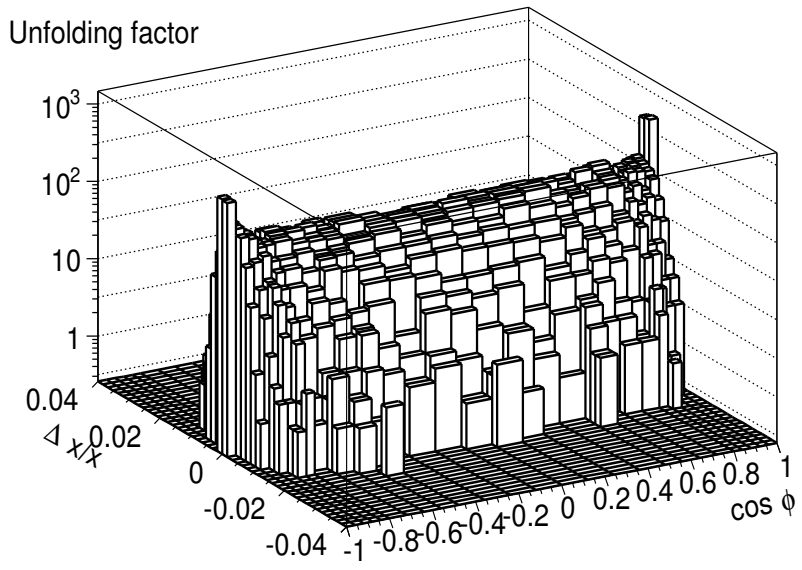

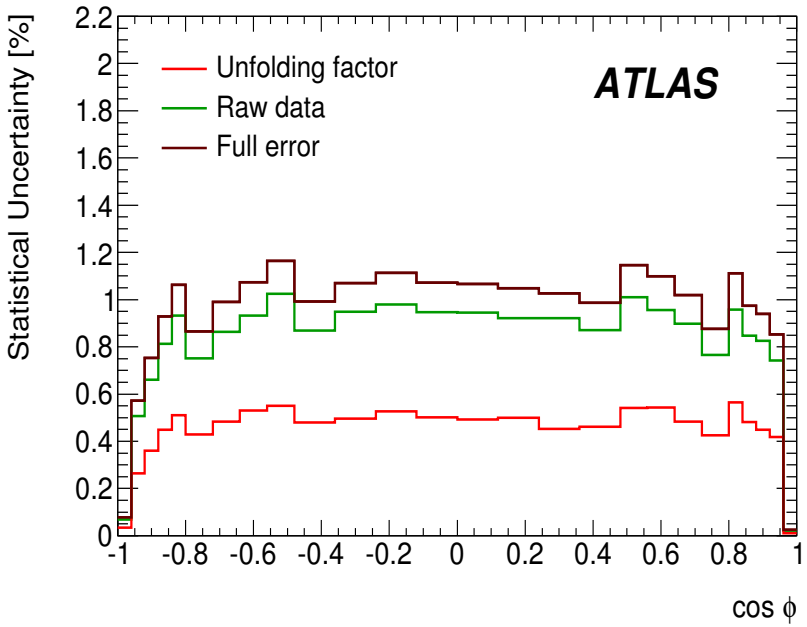

α_s fit results. Nuisance parameters.

Nuisance parameters for TEEC (top) and ATEEC (bottom) and their correlation matrices.